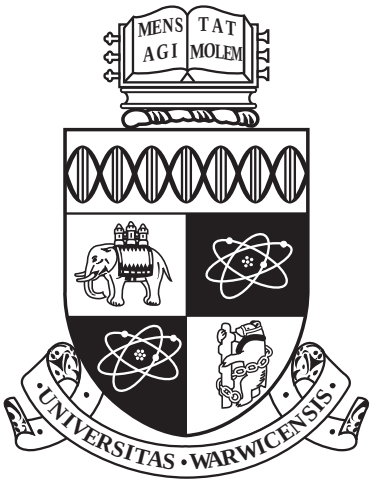

Thermoelectric Transport in the Quantum Hall Regime

by

Poppy Asman

Thesis

Submitted to the University of Warwick

for the degree of

Doctor of Philosophy

Department of Physics

October 2017

THE UNIVERSITY OF
WARWICK

Contents

List of Figures

Acknowledgments

I would like to take this opportunity to firstly thank my supervisor Dr Nicholas d'Ambrumenil for his continued support and help with this work. As well as thank Prof. Julie Staunton for the time she gave me throughout my four years at Warwick.

I would also like to thank my office mates, especially Dr Michael Ambler, and who was happy to have me bounce ideas off of him throughout our time together.

My biggest thanks though will go to my family, who have supported and encouraged me to keep going when I felt myself flagging. Without them behind me, I do not believe I would have finished this work. And finally I would like to thank my son for his understanding throughout all the times I had to work at home, and his commitment to making sure I managed to get my work done.

Thank you all so much for the support I have received throughout the last four years.

Declarations

This thesis is submitted to the University of Warwick in support of my application for a doctorate of philosophy. It has been written and compiled by myself and has not been submitted as part of another degree. All work contained within this thesis is done by the author excluding:

- the experimental data used for comparison which was published in W. E. Chickering, J. P. Eisentein, L. N. Pfeiffer and K. W. West, Thermoelectric response of fractional quantized Hall and reentrant insulating states in the $N = 1$ Landau level. *Phys. Rev.* B, 87,2013.
- The simple model used as a starting point published in N. d'Ambrumenil and R. H. Morf. Thermopower in the Quantum Hall Regime. *Phys. Rev. Lett.* 111, 2013.

Abstract

This research develops a theoretical model to explain the behaviour of the thermopower in the quantum Hall regime. It uses the concept that at low temperatures the transport through the system will be caused by thermal activation as well as that caused by the conductance.

The model is built up in stages, starting with proving the assumption that Dykhne's theorem will work for an asymmetric distribution of particle transport through the system and deriving the behaviour of the particles in the edge states of the system. It then combines this information with a previously developed simple model for the bulk of the modulation-doped GaAs/AlGaAs heterostructure and compares this with experimental data. This reveals that this simple system is not a viable model to represent the data, and as such the model is made more complex with the inclusion of tunnelling.

The different parameters which describe the model are found, the saddle energy gap Δ, the transition value for the edge states c, the current splitting parameter α and the tunnelling parameter γ. This is done either by extracting them from the experimental data, or in the case of α considering it as a free parameter. How these values vary with the temperature is investigated before a comparison of the theoretical model including tunnelling is conducted with the experimental data.

The result from the comparison show a promising alignment between the model and experiment, and further work is proposed where α is no longer considered a constant.

Chapter 1

Introduction

In 1980 it was discovered by Klaus von Klitzing that at high magnetic fields the Hall resistance in semi-conductors, which had previously been believed to be continuous, was in fact quantised. This quantisation appeared in the form of plateaus at the point where the Landau levels were full [1]. This is the discovery that led to the theory of the integer quantum Hall effect. With better quality of semi-conductors, it was found by D. C. Tsui, H. L. Stormer, and A. C. Gossard that these plateaus did not only appear when the Landau levels were full but also between them [7]. This new quantisation gave rise to a whole new area of physics to investigate, including the concept of particles with fraction statistics and fractionally charged quasiparticles [2]. This phenomena became known as the fractional quantum Hall effect. Thirty seven years later and these effects are still very much at the forefront of condensed matter research. The quantum Hall effect is still providing new and varied information on the particles and how they interact with each other and the understanding of how particles behave in this regime, where they are subjected to low temperatures and high magnetic fields is being revealed.

This thesis will focus on developing a detailed understanding of the complex behaviour of the particles in the fractional quantum Hall regime with relation to the thermopower, as this phenomena can give a greater insight into the particles states. Specific attention is shown to those states with an even filling factor, as these are the factors which, as of yet, do not have a completely defined model to explain their presence. This thesis presents a model which could explain these factors' appearance at the low energies in the quantum Hall regime.

The remainder of Chapter 1 will go into the theoretical background, giving a concise explanation of all the physical theories that have been investigated within this thesis. Chapters 2 and 3 explore the experimental results of the inves-

tigation into the thermopower at low temperatures and high magnetic fields, and the proposed theoretical model to explain this behaviour. They will give detailed information on both, as well as discuss the assumptions and limitations with the theoretical model proposed. This will lead to chapter 4 which will show that the main assumption is indeed correct, and can be used in the model. Chapter 5 will investigate the edge states and derive an equation for how the current moves through them in the quantum Hall regime. It will also investigate how that current behaves under various limits to confirm it conforms to the current understanding of physics. The edge current will then be included with the one from the bulk of the material developed in the model from chapter 3, and the thermopower of that system will be investigated in chapter 6. Chapter 7 will then take the investigation further and see how tunnelling will affect the simplified model in Chapter 6. The thesis will be rounded off in chapter 8 by a discussion of the model developed and how it relates to the experimental results, as well as how it could be improved upon in the future and its uses.

1.1 The Hall Effect

The classical Hall effect, discovered in 1879 by Edwin Hall, is the basic foundation of the quantum model. It explains the relationship between the particles in a semiconductor and how they move when subjected to a magnetic field. The theoretical principle is derived from the Lorentz force acting on conduction particles in the material. This is given by

$$\mathbf{F} = -e\mathbf{v} \times \mathbf{B}, \tag{1.1}$$

where e is the charge of the particle, $\mathbf{v}$ is the average velocity of the particles as they travel through the electric field, and $\mathbf{B}$ is the external magnetic field [8]. Therefore from (1.1), it can be shown that when subjected to a magnetic field $\mathbf{B}$ and perpendicular current density $\mathbf{j}$, the particles in the material create an electric field $\mathbf{E_H}$ in the third perpendicular direction [9]. This electric field is given by

$$\mathbf{E_H} = R_H \mathbf{B} \times \mathbf{j}, \tag{1.2}$$

where R_H is the Hall coefficient. This means the particles move across the material in the direction that is perpendicular to both the current and the magnetic field due to the Lorentz force, which is countered by the electric field such movement generates. This is shown in fig. 1.1.

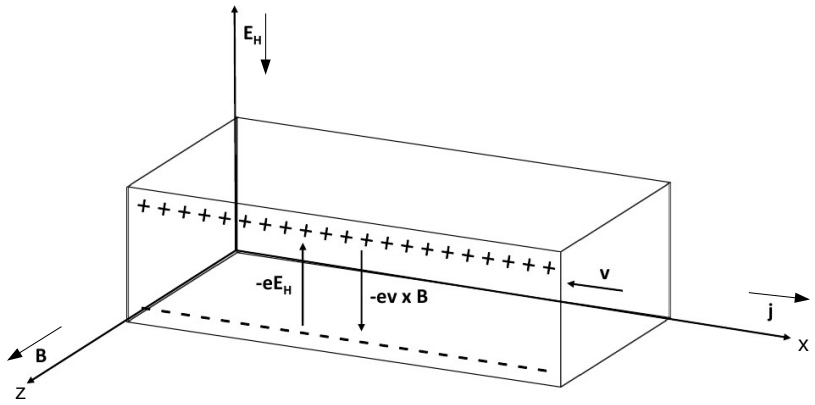

Figure 1.1: A sketch showing the movement of negatively charged particles being subjected to the high magnetic fields.

The Hall effect is easily seen in experiment, where the measurements are taken using the Hall bar geometry, see fig. 1.2. Experimentally it is the Hall voltage V_H that is measured, for given values of current I, and magnetic field $\mathbf{B}$.

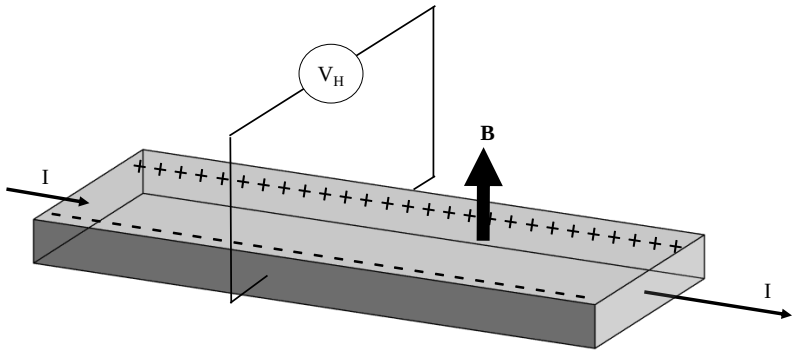

Figure 1.2: A sketch showing the layout of the Hall bar geometry.

This geometry is also used in current experiments to measure the quantum Hall effect as it is the easiest way to conduct research into this phenomena, although the systems studied are much smaller.

1.2 The Quantum Hall Effect: QHE

The quantum Hall effect appears in the 2 dimensional electron gas (2DEG) which lies between two semiconductors in a doped heterostructure [10]. The 2DEG is a scientific model that is used to describe the freedom of movement the electrons have in two dimensions, while being strictly confined in the third [2]. This is shown in fig.

1.3. For the effect investigated here, this means that the electrons can only move in the directions perpendicular to the magnetic field.

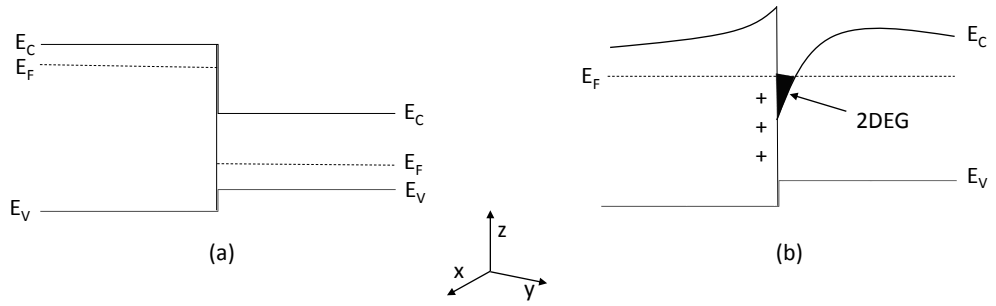

Figure 1.3: Energy levels of a semiconductor heterostructure interface (a) before, and (b) after the charge transfer.
E_C is the energy of the conduction band, E_V the energy of the valence band, and E_F the Fermi energy. The 2DEG can only move in the x-y plane, and not in the z direction.

The quantum Hall effect also only appears at very low temperatures and high magnetic fields. When these conditions are met then plateaus appear in the Hall resistance graph at the points of Landau quantisation (see fig. 1.4). These plateaus are caused by the 2DEG within the system becoming an incompressible quantum liquid [6]. They appear at certain filling factors ν, which are given by

$$\nu = \frac{n_e}{\phi_B}, \tag{1.3}$$

where n_e is the electron density and ϕ_B is the magnetic flux density. The filling factor ν can take on certain integer and rational factional values, and these are defined by the theories of the quantum Hall effect, both integer and fractional.

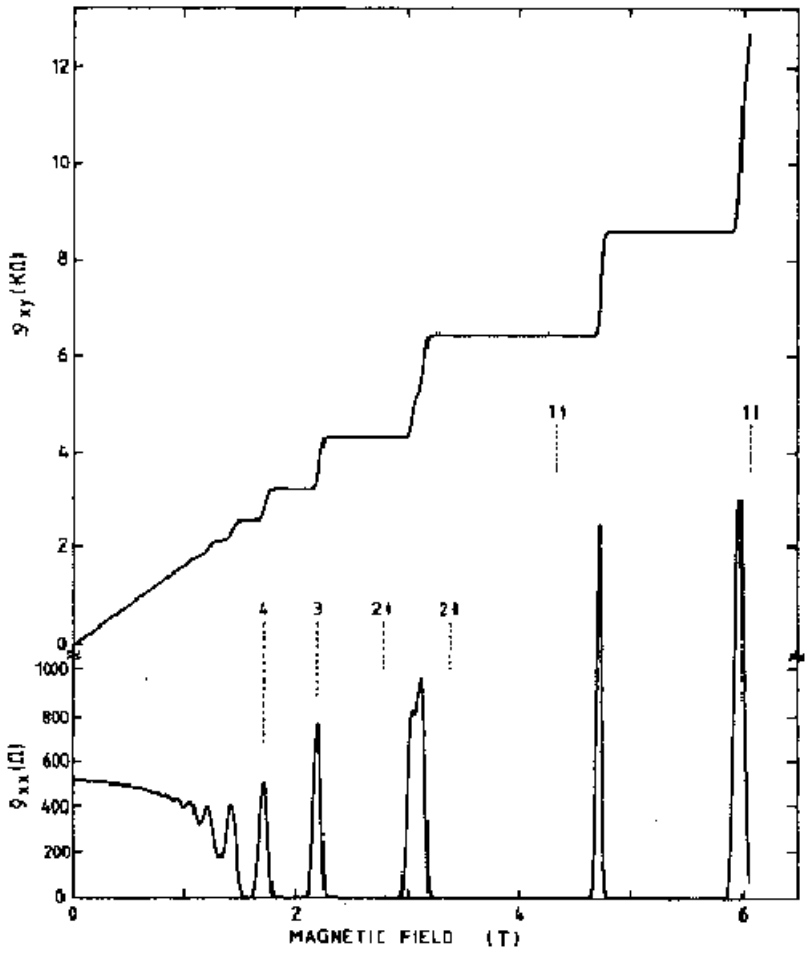

Figure 1.4: The graphical results obtained by Klaus von Klitzing in 1980, showing how the Hall resistance and the dissipative resistance quantises in the quantum Hall regime of low temperatures and high magnetic fields [1]. The top line of data is the Hall resistance, and the bottom set is the dissipative resistance.

It can be seen that where there is a plateau in the Hall resistance the dissipative resistance tends to zero. In fig.1.4 this is where the numbers are shown that correspond to the plateaus in the Hall resistance and the dips in the dissipative resistance, for example the large plateau around 4T where the number 1 is shown. This is because the electrons can now only move in the direction of the dissipative current, which is the direction given by the electric field rather than the magnetic. The filling factors that the plateaus appear at are defined by the quantisation of the conductance, σ, such that it is given by

$$\sigma = \nu \frac{e^2}{h}. \tag{1.4}$$

1.2.1 Landau Quantisation

Landau quantisation is when the electrons in the 2DEG quantize into Landau levels, which are the degenerate, discrete energy levels for the cyclotron orbits [11]. The effects of Landau levels are only seen when

$$k_B T << h\omega_c, \tag{1.5}$$

where k_B is the Boltzmann constant, T is the temperature, h is the Plank constant and $\omega_c = eB/m$ is the cyclotron frequency. From this it can be seen that the quantisation only happens when the temperature is low and magnetic field is high [9]. The difference between two Landau levels is given by $\hbar\omega_c$. Therefore in a pure system, the Landau quantisation will give an energy-density of states relationship shown in fig 1.5a. But the system in which the quantum Hall effect appears is not a pure one. It has disorder from the impurities needed for the 2DEG to form. These impurities give rise to a broadening of the Landau levels into areas where the states are localised, shown in fig. 1.5b.

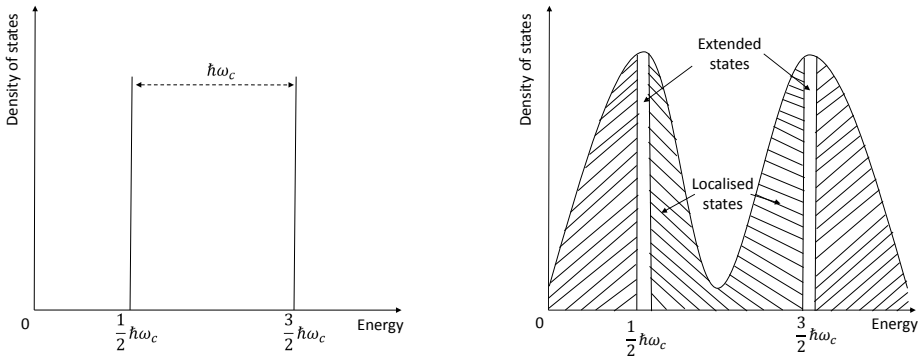

(a) The energy levels for the density of states is clearly defined in a system without impurities.

(b) The Landau levels broaden in a system with impurities, causing areas of localised and extended states.

Figure 1.5: The relationship between the Landau energy levels and the density of states in a 2DEG with (a) a non-doped system, and (b) a system containing impurities.

What this means is that the particles in the localised areas are confined to travel along the contours surrounding the disordered potential, which has peaks and troughs produced by the impurities. Those in the extended states however move freely through the material. These extended states only appear in the areas between the peaks and troughs in the disorder potential, and are the ones which give the

freedom of movement to the particles that results in the Hall resistance, this is shown in fig. 1.6 [2]. It can also be seen experimentally in [12].

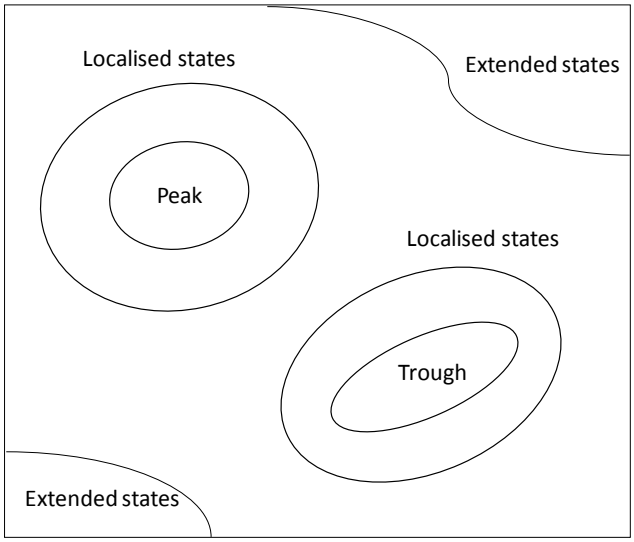

Figure 1.6: A sketch of the trajectories of the particles in both localised and extended states [2].Therefore it can be seen how those in the localised areas move around the peaks and troughs, while those in the extended areas move freely through the material.

1.2.2 The Integer Quantum Hall Effect: IQHE

The integer quantum Hall effect happens when the filling factor is an integer value. It was the first example of the QHE to be seen. Therefore it has been the most widely studied, and is now well understood. There is a well structured model that explains this phenomenon. The concept of which is that the integer quantum Hall effect appears when the Fermi level of the material is situated symmetrically between the extended states of the Landau levels [13], (discussed in section 1.2.1). The levels need to be occupied such that the lower state is completely full, and the higher one still completely empty[14]. This is shown in fig.1.7. From this it can been seen clearly that when this situation is realised, the particle in the lower extended state n, would not be able to move. And the higher extended state of $n+1$ is at a too great an energy for any particle to move up into it. Therefore the 2DEG becomes incompressible and the plateau forms in the resistance graph at this point. Then as the magnetic field is increased the Fermi level will move up and particles will again have the energy to move into the empty state, causing them to once again

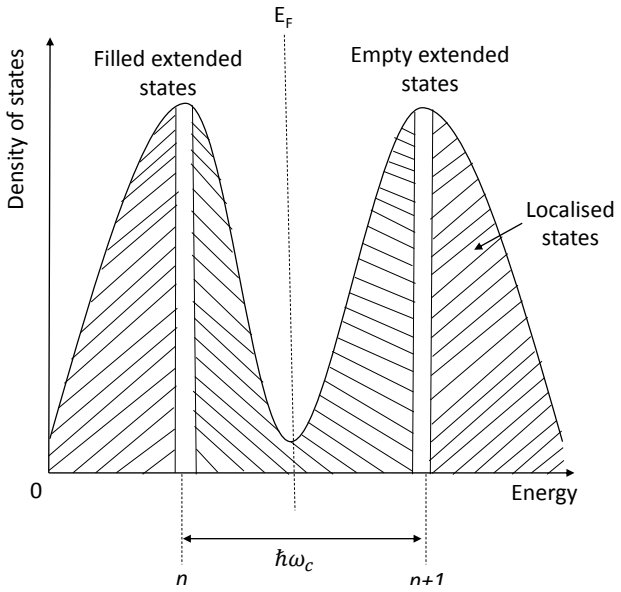

Figure 1.7: The Landau energy picture including the position of the Fermi level for the IQHE to cause the plateaus in the resistance.

traverse the material. This movement causes the plateau in the resistance graph to disappear, until the next integer filling factor where the Fermi level in once again symmetrically positioned between the filled and empty extend states. This carries on and is the physical concept behind the integer quantum Hall effect.

1.2.3 The Fractional Quantum Hall Effect: FQHE

The fractional quantum Hall effect (FQHE) is when the filling factor takes on a rational fractional value. So the conductance equation (1.4) for the system is given by

$$\sigma = \nu \frac{e^2}{h}, \quad \text{where} \quad \nu = \frac{p}{q}. \tag{1.6}$$

This phenomena comes from the electron-electron interaction within the system, otherwise known as the Coulomb interaction. This is why it can appear in areas where there are partially filled extended states [15]. Therefore at certain fractional values of ν, the Coulomb interaction between the particles in different localised states, becomes greater than the interaction with the disorder potential. This causes the electron to de-localise, and move from its orbit around the peak (or tough), onto a trajectory through the material. These trajectories give extended states in areas that are not just at the centre of the Landau level, and in these de-localised extended states the particles can condense into a new many-body incompressible state [16]. It

is these incompressible states that give the plateaus that appear at fractional values of ν [2].

In 1983 R. B. Laughlin proposed a theoretical model to explain how and why these fractional states appeared. The main basis of which is that the particles come together to form quasiparticles which hold a fractional charge, qe, of

$$qe = \frac{e}{q}, \quad \text{for} \quad \nu = \frac{1}{q}. \tag{1.7}$$

These quasiparticles then form the new ground state for his model. He proposed that all other fractional states could be formed from these $1/q$ ground states [17]. Quasiparticle is a term used to define a collection of particles in a strongly correlated system. In such a system the individual particles no longer behave as would be predicted using standard perturbation theory. Instead it is found that the collection of particles will interact weakly with other collections of particles. Thus, the particles behave collectively as single particles would, though the fundamental properties of these quasiparticles are different. They can take on fractional values of those of true particles [18]. The particular quasiparticles believed to be the cause of the FQHE are called composite fermions, which can have fractional charge, and obey the laws of fermionic physics.

Laughlin's theory was expanded by B. I. Halperin in 1984 to include fractions other than those of $\nu = 1/q$. This gives a well defined structure for the quantum Hall effect at odd fractions, which were the only fractions that had been seen at this time [19]. But in 1987, due to the improvement in the quality of the samples being studied and the temperatures that the experiments could be taken to, an even fractional quantum Hall state at value of $\nu = 5/2$ was discovered [20]. The issue with this discovery is that Laughlin's original model does not include the concept of even fractions within it. Therefore a new model needs to be devised that will encompass all the possible fractional quantum Hall states, both even and odd.

The discovery of this model has presented a challenge. As investigation into the even fractional states continued, and further information about them was discovered, the suggestion that the even states are non-Abelian was put forth [21]. This is of interest to many as it would open up the idea of investigating this exotic area of physics, but it has yet to be proved. Instead many have strived to find a viable theory that includes both the odd and even fractional filling factors, as well as agreeing with the experimental results that have been obtained. This is the aim of this thesis, though the model is using the concept of the thermopower rather than the resistance and conductivity of the system. This is done in the hopes that

it simplifies the complex physical system, and that through this, more information about the even fractional states can be determined [6].

1.3 Thermoelectric Transport

The thermoelectric effect describes how heat gets turned into electricity. It is an overarching concept which contains within it three different physical effects. The one investigated in this thesis is the Seebeck effect, which is also known as the thermopower, and that it how it will be referenced throughout this work [22]. The thermopower, also known as the thermoelectric transport of a system S, is given by

$$S_{xx} = -\frac{\Delta V}{\Delta T}, \tag{1.8}$$

which in words can be described as the voltage difference, ΔV, needed to make the current zero over the temperature gradient, ΔT, of the material. Therefore this defines the amount of voltage needed to quench the dissipative current that is created by the temperature difference [23]. This can physically be taken as the entropy per charge carrier [24]. The entropy of the states is of great interest in the research of the FQHE [25]. This is due to the fact that if the quasiparticles are obeying non-Abelian statistics, as it has been proposed that the even 5/2 state does [21], then the entropy carried by then will be much higher than that carried by the Abelian quasiparticles at low temperatures [[24],[26]]. As such developing a model that explains the thermopower behaviour for all the filling factors of the FQHE could further the understanding of physics involved in these states.

The thermopower has certain properties, for example it is negative for electrons and positive for holes, as per their charge. Also the dissipative thermopower will reduce at low temperatures where a plateau would occur in the resistor graph. This corresponds to the higher amount of entropy that is present within these states. Therefore the different states of the FQHE will be found within the data obtained. This is shown in Chapter 2 where the results collected in [3] are discussed. This is the data that is used to investigate the thermopower phenomena throughout this thesis, and that which the model developed will be compared to at the end.

Chapter 2

Experimental Investigation of Thermopower

The thermopower is an interesting phenomena as it gives insight into parameters and phases of a material that are not otherwise seen, for example its direct relationship to the entropy of a particle at low temperatures. There are more than one proposed experimental set-up that will allow the investigation of this phenomena, and in this thesis the main two will be discussed and their advantages and disadvantages explained. The two set-ups are the Hall bar geometry, which was explained in chapter 1 and the Corbino geometry. The Corbino geometry is where a ring is used in a Hall experiment rather than the standard bar. In fig.2.1 it is shown how the voltage difference, ΔV, and the temperature difference, ΔT, are measured across the ring of material. Due to this the dissipative current is also measured in that direction, whereas the Hall current travels around inside and does not involve itself in the measurements for the thermopower. Also it can be seen that as the measurements are taken in the radial direction, there will be no edge effects that need to be taken into account when studying the dissipative transport. Therefore only the bulk of the material will need to be modelled to determine the behaviour of the particles within the system. This simplifies the theoretical model needed, as only one behaviour needs to be taken into account. But, it is very hard for experimentalists to create such a prefect ring, and any anomaly in the structure that will cause the slightest variation from a shape in which the radial direction is the only one of interest, will cause a deviation from the theoretical model, which could cause a dramatic difference in the results obtained [27]. The reasoning for this is shown in fig.2.1.

The Hall bar geometry is the opposite. This shape is much easer for the

experimentalists to create, and the measurement of the voltage and temperature differences can be recorded using a system similar to the Hall effect experiments. This is why most experiments are done in this geometry. But it does create troubles for the theoreticians as they have not only the behaviour of the particles in the bulk to explain, but also those on the edges. Though there have been recent developments into experimentally using the Corbino geometry to investigate the behaviour of particles in some Landau levels [28].

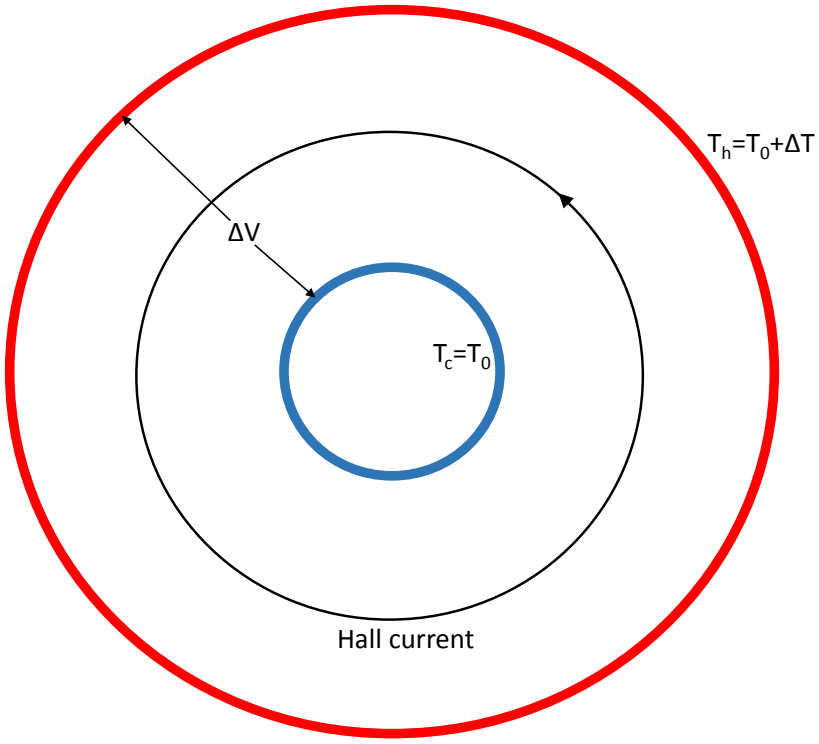

Figure 2.1: A sketch showing the Corbino geometry and how the different parameters are measured using it. T_c is the colder temperature whereas T_h is the hotter side.

2.1 Thermopower at Low Temperatures

As discussed, the thermopower relates directly to the entropy of the individual particles. This was investigated in the paper *'Thermoelectric response of fractional quantized Hall and re-entrant insulating states in the N=1 Landau level'* [3] which threw up some interesting results. It is these results which spurred the idea for this thesis, and is the basis of motivation for the development of the model presented

here.

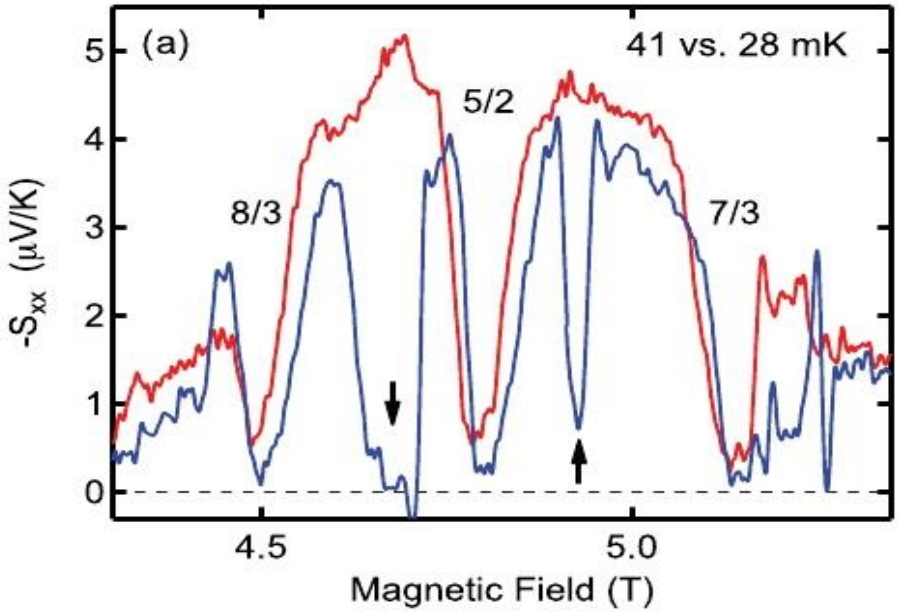

Figure 2.2: This is a image of the data for the thermopower at different temperatures, $red = 41mK$ and $blue = 28mK$, that was obtained by Chickering et al. in 2013 and published in the paper [3].

Shown in fig.2.2 is the relationship between the thermopower S_{xx}, which is represented in the convention of electron dominated transport and thus is negative, and the magnetic field B. There are several things of note shown in this diagram. The first is the fact that at a certain point, the thermopower changes sign at low temperatures. This means that at that particular point the transport domination suddenly switches from electrons to hole domination. This switch does not happen at a magnetic field value that would be associated with a filling factor. In fact there are two different points where the thermopower S_{xx} minimises, but these are not at reconsigned filling factors. It is reasoned in the paper that these minima are due to the re-entrant integer quantized Hall effect (RIQHE), which are non-quantum Hall states [2], these have been seen in behaviour of holes in the N=0 level [[3], [29]] as well as at higher values of N [30], but this has not been proven, and it is something that the model being described in this thesis hopes to be able to explain. But what is of most interest though, is the fact that the thermopower switches sign so abruptly at low temperatures. This confirms the high dependence S_{xx} has upon the temperature, as well as creating an interesting phenomena to study, in the hopes

of deriving a model that would explain this behaviour, and thus gain a step closer to the understanding of the fundamental physics involved in low temperature, high magnetic field physics.

2.2 Theoretical Approach to Explain the Behaviour of the Thermopower at Low Temperatures

The theoretical way to approach modelling the behaviour of the thermopower in the low temperature limits is to look at the temperature dependences of the various transport coefficients in the quantum Hall regime, and find the properties which are directly measurable in experiment. This is interesting as the thermal activation of the carriers is a significant source of error to the quantized Hall conductance [14]. This means that while the thermoelectric effect for the system will be that given by the quantized Hall effect, which has a solid theoretical standing, when measured in low temperature experiments it will also have the input from the thermal effects on the carriers. Both of these will contribute to the movement of the electrons through the material, and therefore on the conductance, and yet they behave in very different manners through the bulk of the sample and around the edges [31]. The next chapter will describe in more detail the model that has been developed to investigate this behaviour in the bulk.

Chapter 3

Theoretical Model

In the model for the dissipative transport proposed in [6], only the bulk of the material is considered as it was derived in the Corbino geometry. Therefore there are no edge state contributions to take in to account. The working principle of this model is that there will be a varying background potential due to the disorder of the sample which comes from the temperature gradient. This disorder will cause compressible regions to form in the incompressible fluid. The dissipative transport will therefore be due to the movement between these regions. This is shown in fig. 3.1 where it can be seen how the thermal activation of the quasiparticles will move them across the incompressible region from one compressible puddle to the other puddle which has a lower temperature, T and chemical potential, μ. The

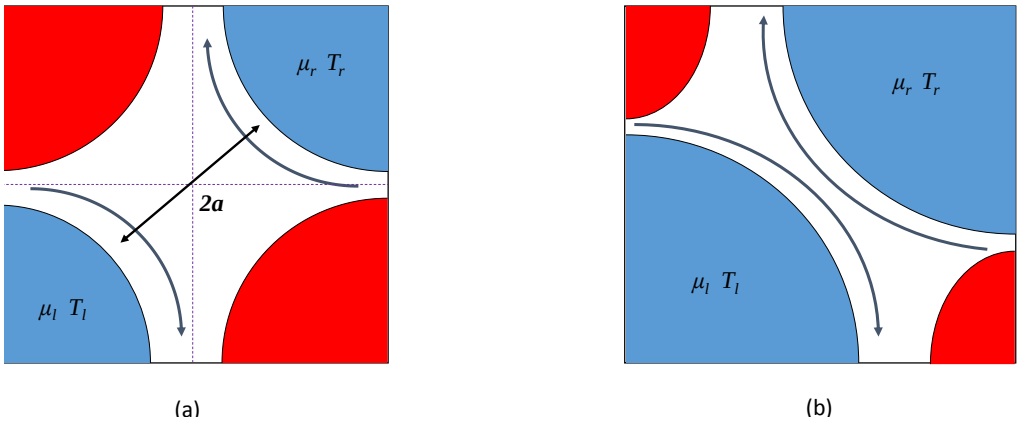

Figure 3.1: How the quasiparticles move through the bulk of the material. The red and blue parts are areas of compressible puddles within the incompressible fluid. The red indicates quasiholes and the blue quasiparticles. The arrows show how the quasiparticles are localised around the puddles.(a) is the situation at minimum dissipative resistance, where $2a$ is the distance between the compressible regions, and (b) shows the arrangement after the quasiparticles have been thermally activated.

incompressible region that the quasiparticles will transverse is known as the energy gap of the material, and can be modelled as a saddle point. This is due to the fact that the quasiparticles will need higher than normal energy to transverse the incompressible region, and they would also need this higher energy to move across a saddle point. This is shown in fig.3.2 which shows the band alignment for the system [6].

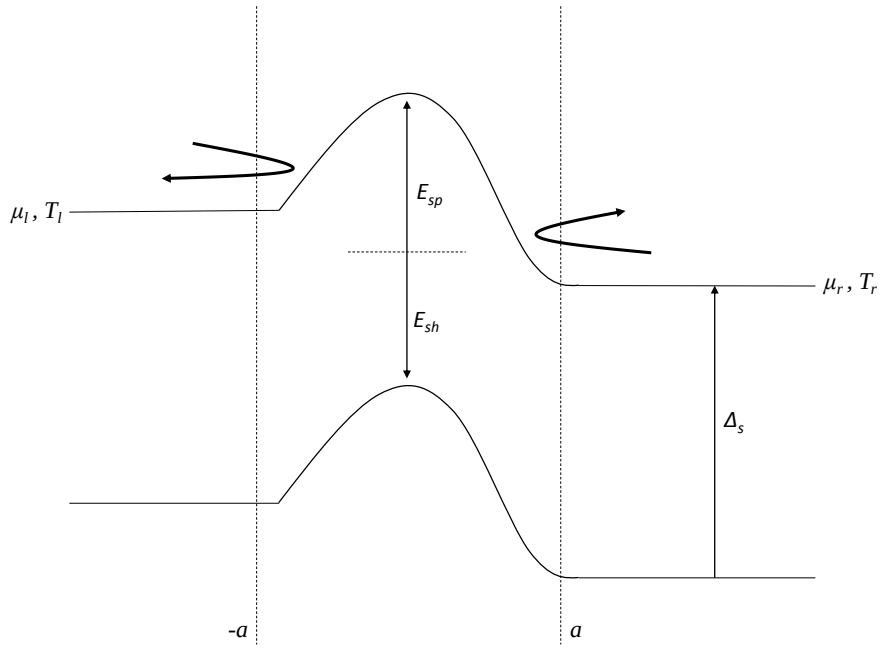

Figure 3.2: A diagram showing the band alignment for the system.The arrows represent how the quasiparticles are moving around the localised trajectories in fig.3.1, and Δ_s is the energy gap for the saddle point. E_{sp} and E_{sh} are the energies needed for the quasiparticles and quasiholes to transverse the saddle point, respectively.

The band alignment of a typical saddle point created by the disorder, has different values of the chemical potential, μ, and the temperature, T, on either side. So the quasiparticles will want to move from the left to the right, which has the lower values. They will either have the energy to go over the barrier or they will tunnel through. This movement will create a flow of charge through the system. This transfer of the quasiparticles across the saddle point will be given by the

$$i_{lr} = \frac{1}{h}\int_0^{\Delta_s} dE\mathcal{T}\left(E - E_{sp}\right)\exp\left(-\frac{E-\mu_l}{T_l}\right) \tag{3.1}$$

where T_l and μ_l are the temperature and chemical potential of the left puddle

respectively. Also the $\mathcal{T}(E - E_{sp})$ is the transmission probability of a quasiparticle crossing the saddle point. For a simplified model that does not take account of tunnelling this value is either 0 or 1. Therefore this gives the net (number) current of the quasiparticles system to be [6]

$$i_s = \frac{1}{h}\left(-(qe)\delta V + \left(1 + \frac{E_{sp}}{T}\right)\delta T\right)\exp\left(-\frac{E_{sp}}{T}\right). \tag{3.2}$$

The same equation can be found for the quasiholes transport as well. The difference for the quasiholes being that the charge, qe, will have an opposite sign, and the whole equation will be negative as the transport will be in the different direction to that of the quasiparticles. The net transfer of the quasiparticles therefore reflect the potential difference ΔV, and temperature difference ΔT that are needed to find the thermopower for the bulk of the material. This is done by using the relation between the current, δV and δT that [6]

$$I = L^{(11)}\delta V - L^{(12)}\frac{\delta T}{T}. \tag{3.3}$$

Therefore the equation for the thermopower can be written using (3.3) such that

$$S_{xx} = -\frac{\Delta V}{\Delta T} = -\frac{1}{T}\frac{L^{(12)}}{L^{(11)}}. \tag{3.4}$$

Using (3.4) and (3.2) will give a thermopower for both the quasiparticle and quasiholes to be

$$S_{xx} = -\frac{\left(1 + \frac{E_{sp}}{T}\right)\exp\left(-\frac{E_{sp}}{T}\right) - \left(1 + \frac{E_{sh}}{T}\right)\exp\left(-\frac{E_{sh}}{T}\right)}{\exp\left(-\frac{E_{sp}}{T}\right) + \exp\left(-\frac{E_{sh}}{T}\right)}. \tag{3.5}$$

To determine the equations that will represent the average saddle point heights for the quasiparticles, E_{sp}^{av} and the quasiholes, E_{sh}^{av} the first thing that needs to be considered is how at the centre of the fractional quantum Hall plateau they are equal, both of them having the value of $E_{sp}^{av} = E_{sh}^{av} = \Delta_s/2$. But as the model moves away from the centre of the plateau, the variation of the quasiparticle and quasihole transport will come into play. This is due to the fact that there will be certain values of saddle point, that the quasiparticles can not transverse, and also points which are the easiest for them to cross. The same must be said for the quasiholes as well. Therefore taking the filling factor to be given by $\nu_m \pm \delta\nu_m$ - where ν_m is the value of the filling factor at the centre of the plateau, then it can be written that E_{sp}^{av} will disappear when $\nu = \nu_m + \delta\nu_m$. And vice versa E_{sh}^{av} will disappear when

$\nu = \nu_m - \delta\nu_m$. If it is assumed that the variation in E_{sp}^{av} and E_{sh}^{av} are linear, then using the variable $g = \delta\nu/\delta\nu_m$ equations that describe the two energy gaps can be written down [6]. Therefore it is given that

$$E_{sp}^{av} = (1-g)\,\frac{\Delta_s}{2} \qquad \text{and} \qquad E_{sh}^{av} = (1+g)\,\frac{\Delta_s}{2}. \tag{3.6}$$

Across the whole of the material there is a network of these saddle points due to the background potential. They can be modelled as a chessboard style potential as seen in fig.3.3. This chessboard potential can then be modelled as two networks of resistors. One for the quasiparticles, and one for the quasiholes. The resistor values in this network are determined by the saddle point heights [4]. This model assumes

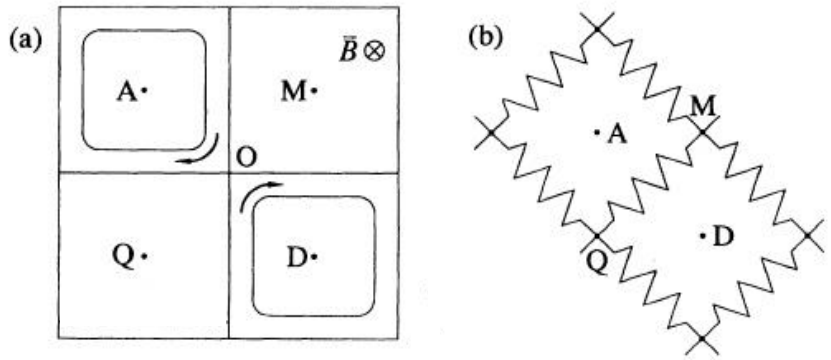

Figure 3.3: a sketch of the chessboard potential layout taken from [4]. O is the saddle point, A and D are the centres of the two quasiparticle regions and M and Q are the centres of the quasihole regions. a) shows the saddle point modelled as a chessboard potential, and b) shows how they are modelled as resistors for the quasiholes region. relating these diagrams to fig.3.2 A is the region that corresponds to being on the left of the saddle point, O is the region in the centre that is the saddle point, and D is the region to the right of the saddle point.

that as the conductance of the saddle points is given by an exponential, and that the saddle points can be modelled as a network of resistors, then Dykhne's theorem [32] can be used to find the average value for the system. This theorem states that the effective conductance of a network of resistors which have their natural log values symmetrically distributed will be given by the mean value of the resistors[6].

$$\ln \sigma_{\text{eff}} = < \ln \sigma > . \tag{3.7}$$

The problem with using this assumption is the fact that the values of the resistors

will not be symmetrically distributed due to tunnelling effects at low temperatures. Therefore it needs to be investigated if this assumption still holds for a situation where the distribution is slightly asymmetric. Also to compare this model with the experimental data found in [3] and discussed in chapter 2, then the edge effects need to be included as that experiment was conducted in the Hall bar geometry, whereas this model is currently in the Corbino geometry.

Chapter 4

Assumption: Dykhne's Theorem

In 1971 A. M. Dykhne published a paper on the conductivity of a two-phase thin film with a random distribution of the phases. It discussed how this overall conductivity is equal to the geometric mean of those of the two phases, as long as their concentration is the same [32]. This means that as long as the range of varying phases throughout the system is symmetrical, the equation for the geometric mean can be used to find the total conductivity of said system. This is due to the fact that the conductivity can be represented in a logarithmic way, which is found to be additive upon mixing [32]. In this paper he also applied his theory to different dependences for the conductivity, including the smooth dependence of the conductivity on coordinates, saying that as long as the system being looked at is symmetric then

$$\sigma_{\text{eff}} = \exp \langle \ln \sigma \rangle \tag{4.1}$$

will be true. For a Gaussian distribution he showed that the effective conductance would have the form

$$\sigma_{\text{eff}} = \langle \sigma \rangle \exp(-\Delta^2/2) \tag{4.2}$$

where Δ is the root mean square of the fluctuation of the logarithmic conductivity [32]. This means that if the system being looked at has fluctuations that are minimal, then it can be taken that $\exp(-\Delta^2/2) \approx 1$. This gives

$$\sigma_{\text{eff}} \approx \langle \sigma \rangle \tag{4.3}$$

which is the mean of the conductance of the system. For a symmetric system this mean is simplistically given by

$$\langle \sigma \rangle = \frac{\sigma_{\max}}{2}. \tag{4.4}$$

Therfore (4.1) can be rewritten such that

$$\frac{\sigma_{max}}{2} = \exp\langle \ln \sigma \rangle \,. \tag{4.5}$$

This will also work for a network of resistors as

$$\sigma = \frac{1}{R}, \tag{4.6}$$

and therefore replacing (4.6) in (4.1) the result becomes

$$R_{\text{eff}} = \exp\langle \ln R \rangle \tag{4.7}$$

which due to (4.4) will become

$$\frac{R_{\text{max}}}{2} = \exp\langle \ln R \rangle \,. \tag{4.8}$$

As stated in chapter 3, it is possible to model the saddle point potentials in the compressible puddles of the model as a network of resistors [33]. For example as in a chessboard potential [4]. Therefore as long as the system of saddle points is symmetric then Dykhne's theorem will hold. But the system discussed in chapter 3 is one of a slightly asymmetric distribution which has a flat plateau in the centre and then diverged up and down at the edges due to tunnelling, shown in fig.4.1.

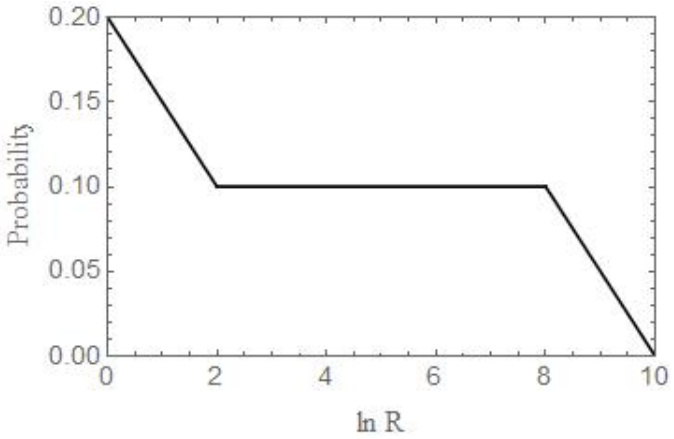

Figure 4.1: A diagram showing the real potential for the model in this thesis.

The question addressed in this chapter is whether the assumption that Dykhne's theorem can be used for this asymmetric potential, is correct. To do this, the transfer matrix approach is discussed as a way to study the conductance of a random disordered system in simulation.

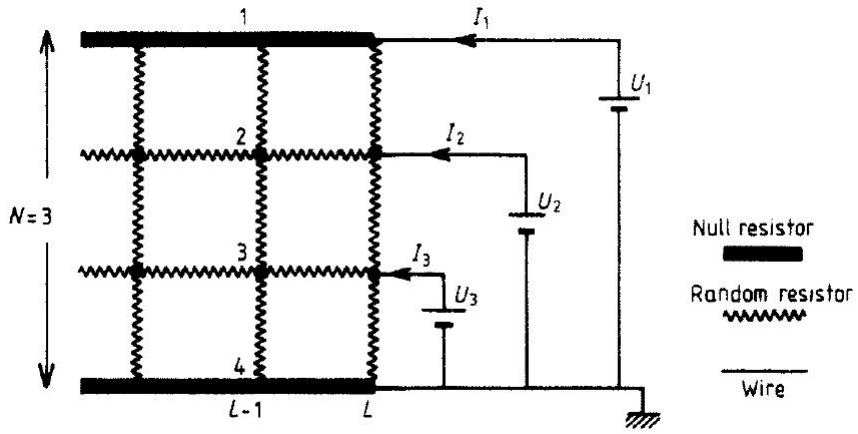

Figure 4.2: The layout of the lattice with no resistance added [5].

4.1 Transfer-Matrix Approach

The transfer-matrix formulation was introduced by B. Derrida and J. Vannimenus in 1982 as a way of finding the exact solution for the conductance of a disordered system [5]. It was developed for a network consisting of long strips with resistors placed at random on a square lattice. The initial situation for this system is the one where there is no resistance upon the lattice, [Fig. 4.2], which is governed by the matrix equivalent of Ohm's law,

$$\begin{pmatrix} I_1 \\ I_2 \\ \vdots \\ I_N \end{pmatrix} = A_L \begin{pmatrix} U_1 \\ U_2 \\ \vdots \\ U_N \end{pmatrix} \tag{4.9}$$

where A_L is the matrix that characterises the effect of the transfer-formulation. Therefore this is the matrix which will change for every column of resistors added to the network. The response to handling this situation is to use the concept of the transfer-matrix approach, which is to transfer from the Lth column to the $(L+1)$th column by adding the horizontal, h_i, and vertical, v_i, resistors. These resistors are added in the configuration shown in Fig. 4.3.

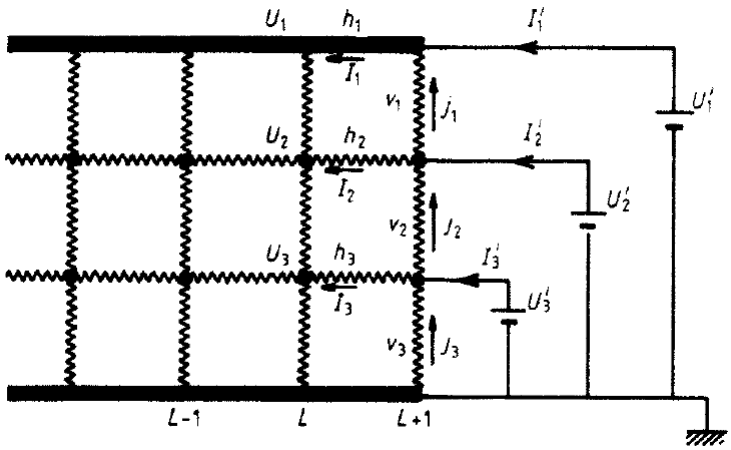

Figure 4.3: The network of resistors showing the addition of the vertical, v_i, and horizontal, h_i, resistors to the $(L+1)$th column. It includes how the current and voltage are shown in the network [5].

From Fig.4.3 it can be seen that (4.9) can then be written in the form of the new current, I_i', and voltage, U_i', such that it becomes

$$\begin{pmatrix} I_1' \\ I_2' \\ \vdots \\ I_N' \end{pmatrix} = A_{L+1} \begin{pmatrix} U_1' \\ U_2' \\ \vdots \\ U_N' \end{pmatrix}. \tag{4.10}$$

Therefore $\mathbf{A}_L$ transforms into the new matrix $\mathbf{A}_{L+1}$ by adding the resistance given from the vertical and horizontal components of the new strip [5]. For ease of calculation only the horizontal resistors will be added first. So by taking the voltages U_i' to be fixed and external we get the relation that

$$U_i = U_i' - h_i I_i \tag{4.11}$$

as $V_i = h_i I_i$ is given by Ohm's law. This equation can be written in matrix form as

$$\mathbf{U} = \mathbf{U}' - \mathbf{HI} \tag{4.12}$$

where

$$H_{ij} = h_i \delta_{ij} \tag{4.13}$$

and $h_1 = 0$ as the top line of resistors are all connected, [Fig. 4.3]. There is also the relation that the currents I_i and the voltages U_i' are related by a matrix $\mathbf{B}_{L+1}$ such

that

$$\mathbf{I} = \mathbf{B}_{L+1}\mathbf{U}'. \tag{4.14}$$

Therefore putting (4.12) into (4.9) then the matrix equation becomes

$$\mathbf{U} = \left(\mathbf{1} + \mathbf{H}\mathbf{A}_\mathbf{L}\right)^{-1}\mathbf{U}' \tag{4.15}$$

and using this result along with (4.14) in (4.9), will lead to the relation that

$$\mathbf{B}_{L+1} = \mathbf{A}_L\left(\mathbf{1} + \mathbf{H}\mathbf{A}_L\right)^{-1} \tag{4.16}$$

which is the horizontal component of $\mathbf{A}_{L+1}$ [5]. If the vertical resistors v_i are now added, using the condition that the voltage is U_i' at site i in the $L+1$ column, then the current through the vertical resistors is given by

$$j_i = \frac{U_{i+1}' - U_i'}{v_i}. \tag{4.17}$$

From this it is seen that the current I_i' through the wire connected to v_i at site $L+1$ is given by

$$\begin{aligned} I_i' &= I_i + j_{i-1} - j_i \\ &= I_i + \left(\frac{1}{v_i} + \frac{1}{v_{i-1}}\right)U_i' - \left(\frac{1}{v_i}\right)U_{i+1}' - \left(\frac{1}{v_{i-1}}\right)U_{i-1}'. \end{aligned} \tag{4.18}$$

Taking $1/v_0 = 0$ this equation is valid for v_1. This gives that the matrix for the vertical resistors. (4.18) can be rewritten as

$$\mathbf{I}' = \mathbf{I} + \mathbf{V}\mathbf{U}'. \tag{4.19}$$

From (4.19) the matrix components for the vertical resistors matrix $\mathbf{V}$ are found to be

$$V_{ij} = \left(\frac{1}{v_i} + \frac{1}{v_{i-1}}\right)\delta_{ij} - \left(\frac{1}{v_i}\right)\delta_{j,i+1} - \left(\frac{1}{v_{i-1}}\right)\delta_{j,i-1}. \tag{4.20}$$

Now using (4.10), (4.14), (4.16) and putting this into (4.19) then this gives the relationship that

$$\begin{aligned} \mathbf{A_{L+1}} &= \mathbf{V} + \mathbf{B_{L+1}} \\ &= \mathbf{V} + \mathbf{A_L}\left(\mathbf{1} + \mathbf{H}\mathbf{A_L}\right)^{-1}, \end{aligned} \tag{4.21}$$

which shows the relationship between A_L and A_{L+1}. This relation is a recurrence

relation. This means that for every column of resistors that is added to the system, the characteristic equation for A_L (4.21) has to be calculated to be used as the next column is added. For a square $N \times N$ lattice we have that the final A_L will be given when $L = N$ and therefore will be denoted by A_N [5]. From this A_N the total resistance of the network can be calculated using (4.9), such that

$$\mathbf{I} = \mathbf{A_N U}, \tag{4.22}$$

which is equivalent to Ohm's Law which states

$$\mathbf{I} = \mathbf{R^{-1} U}, \tag{4.23}$$

and therefore

$$\mathbf{R} = \mathbf{A_N^{-1}}. \tag{4.24}$$

Looking back at Fig.4.3, it can be seen that the current that is effected by the total resistance of the network will be that which travels down the $i = 1$ wire. Therefore the total resistance of the network is given by

$$R = \mathbf{A}_N^{-1}(1,1). \tag{4.25}$$

Using this process it is possible to confirm Dykhne's Theorem (4.8) for a system with a square lattice network.

4.2 Dykhne's Theorem using the Transfer-Matrix Approach

The approach shown in section 4.1 can be used to find the effective value for the resistance using Dykhne's theorem. To do this the system of resistors must be a symmetric lattice. Therefore the characteristic matrix A_L must be $n \times n$ and therefore the number of recursions for the system will also be n. As such the result of R will then obey (4.8). This then leads to the fact that the higher the value of n the more precise the result for R should be. If these parameters are adhered to then a program can be written which will repeat this process for random values of h_i and v_i giving the total value of R for a given $n \times n$ system. These results can then be plotted, and the effective resistance can be found and checked against Dykhne's theorem. The higher the number of iterations of the program, the greater the accuracy of the results.

This process is shown in sections 4.2.1 and 4.2.2 for systems with a particular configuration of resistors that is dictated by their symmetric probability distributions. In sections 4.2.3 and 4.2.4 linear asymmetric systems are looked at, to see how the values given by the left and right hand sides of (4.8) differ for this change. This is done to see if it is correct to use the assumption stated in the theoretical model in chapter 3. In all these sections the probability distributions are analysed for the natural logarithmic resistance, $\ln R$, rather than R alone. Therefore (4.8) for a symmetric distribution will become

$$\frac{\ln R_{\max}}{2} = \langle \ln R \rangle \,. \tag{4.26}$$

4.2.1 System with a Symmetric Top Hat Probability Distribution

The first system looked at is a normal, top hat probability which is symmetric, and will be given the values which range between $[0, \ln R_{\max}]$. This is shown in fig.4.4a. This distribution means that the current can run through each value of resistance with equal probability, and as such can hold any value between $\ln R_{min}$ and $\ln R_{max}$. As such this is being looked at so that it can show a robust confirmation that Dykhne's theorem does indeed hold. Using the transfer-matrix approach shown in section 4.1 for two different $n \times n$ matrices it is possible to produce a distribution graph for the network of resistors, as shown in fig.4.4b.

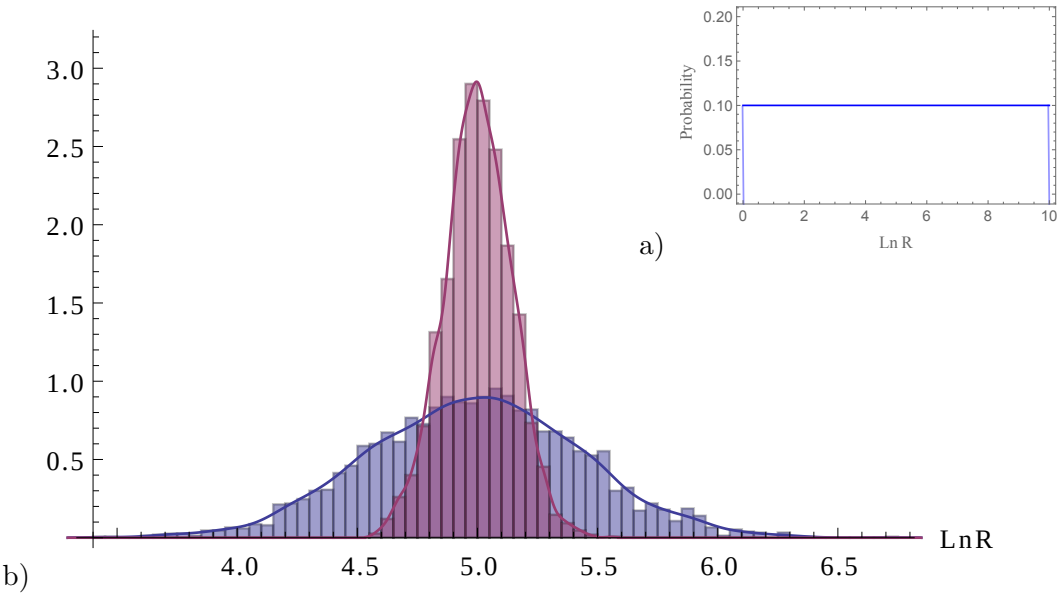

Figure 4.4: a) The top hat probability being looked at. b) The distribution of the values of $\ln R$ for a range of $[0, 10]$. The blue shows the distribution for a 10×10 matrix and red for a 30×30 matrix, running over 3000 iterations.

For the range of $\ln R$ being $[0, 10]$ and the distribution being symmetric, then the theoretical natural log of the effective resistance, $\ln R_{\text{theo}}$, will be given by

$$\ln R_{\text{theo}} = \frac{\ln R_{\text{max}}}{2} = 5. \tag{4.27}$$

For 3000 iterations, the program gives that the two matrices have values for the natural log of the effective resistance, $< \ln R_i >$ - where the i subscript will be the notation used to differentiate between the different sized matrices being looked at, i.e R_{10} is the resistance for the 10×10 matrix, and R_{30} is the resistance for the 30×30 matrix, to be

$$\langle \ln R_{10} \rangle = 4.96752, \qquad \langle \ln R_{30} \rangle = 5.00005 \tag{4.28}$$

which are very close to the value predicted by (4.27). The differences in the values are

$$\Delta_{10} = \ln R_{\text{theo}} - \langle \ln R_{10} \rangle = 0.02479 \tag{4.29}$$

$$\Delta_{30} = \ln R_{\text{theo}} - \langle \ln R_{30} \rangle = 0.00005, \tag{4.30}$$

which are within a standard deviation, σ, from the mean value as

$$\sigma_{10} = 0.44846, \qquad \sigma_{30} = 0.13994. \tag{4.31}$$

Therefore from these values it is seen that Dykhne's theorem does indeed give a good approximation for the value of the effective resistance for this system. Also from the above numbers it is seen that as the value of n increases, then the standard deviation reduces. This shows that the larger the resistor network the more precise the value of the effective resistance is going to be, which is to be expected. This is shown more significantly in fig.4.5 where it can be seen that at around the value of $n = 25$ the standard deviation stops changing, having reached the limit of precision that can be achieved using the parameters stated. This shows that it is not needed to go higher in matrix size, to gain a more precise result, as above this point the precision will be the same. From this it is seen that it is true that Dykhne's theorem will get more precise the larger the network of resistors being looked at. Therefore this theorem holds very well for a large system of resistors.

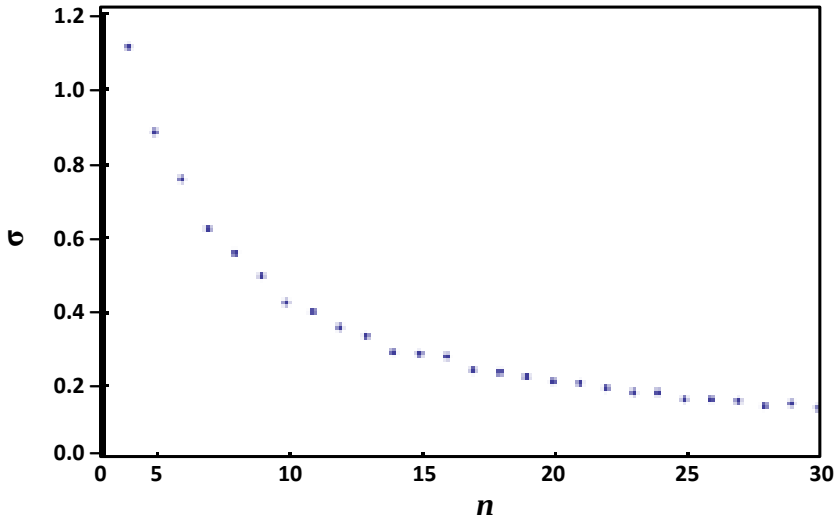

Figure 4.5: How the standard deviation, σ, changes with the changing size of the $n \times n$ matrices for the range of the values of $\ln R$ being $\ln R_{max} = 10$, running over 1000 iterations.

The last relationship that needs to be considered is how the standard deviation changes with different maximum values of $\ln R$, to see how this affects the accuracy of Dykhne's theorem. It can be seen from fig.4.6 that the standard deviation increases as you increase the value of $R_{\max}$. This increase is not a linear relationship but slightly curved. Therefore at lower values of $\ln R_{\max}$ the standard deviation changes less than at higher values. Thus the more accurate the theorem is at these lower levels.

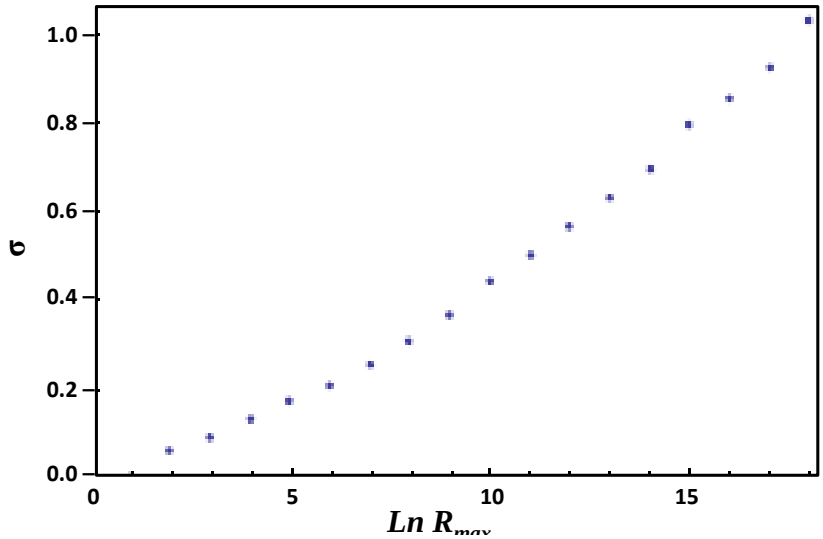

Figure 4.6: How the standard deviation σ changes with an increasing value for $\ln R_{\max}$ for a 10×10 matrix system, running over 1000 iterations.

From the above analysis it can be seen that Dykhne's theorem does indeed apply for both small and large systems, and it can be used for all ranges of $\ln R$ as well. This proves its ability to perform the calculations required for a symmetric system, and determines that it is indeed a viable theorem for this type of model. The theorem will next be tested against another symmetric distribution, but this is not a normal one.

4.2.2 System with a Symmetric, Double-Delta Function Probability Distribution

In this system $\ln R$ can take one of two values with equal probability. The two choices are zero or $\ln R_{\max}$. As this is a symmetric distribution then it should still obey Dykhne's theorem where the theoretical effective $\ln R$ is given again by

$$\ln R_{\text{theo}} = \frac{\ln R_{\max}}{2}. \tag{4.32}$$

Using (4.32) where $\ln R_{\max} = 10$, the effective resistance is once again

$$\ln R_{\text{theo}} = 5. \tag{4.33}$$

Using the transfer-matrix approach to produce random numbers which are then assigned to one of the two delta functions gives fig.4.7b. From this it can be seen that the higher the value of n, the closer to the effective value (4.33) the peaks of

the distribution will become.

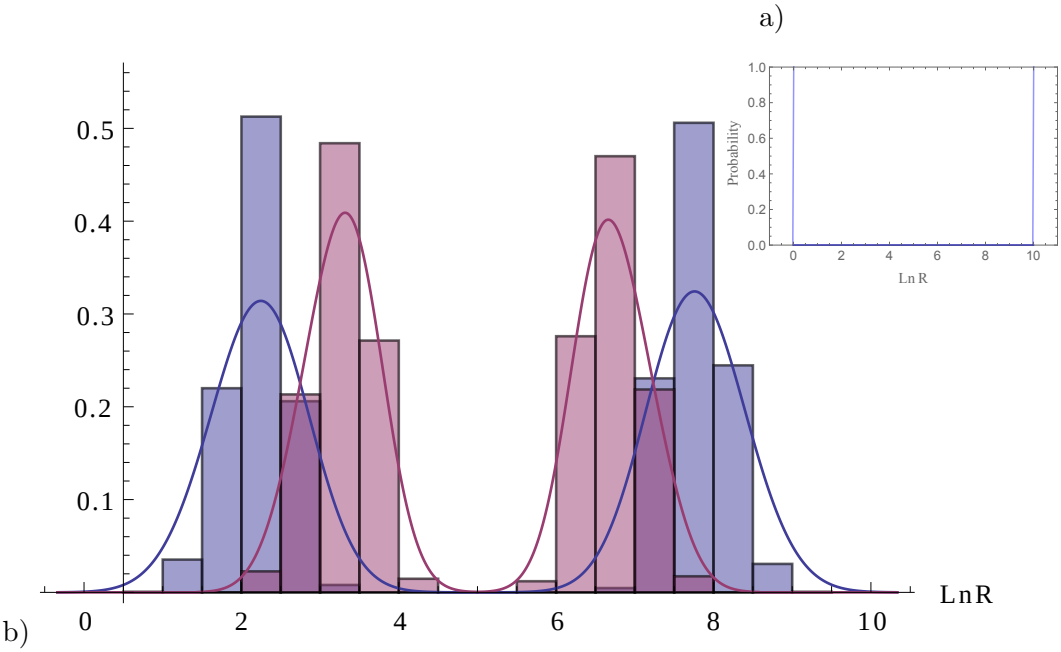

Figure 4.7: The distribution of $\ln R$ for a range of $[0, 10]$ for the system with two delta functions. The blue shows the distribution for a 10×10 matrix and the red the distribution for a 30×30 matrix, running over 3000 iterations.

The program gives, over 3000 iterations, the values of $\ln R_{\text{eff}}$ to be

$$\langle \ln R_{10} \rangle = 4.16947 \qquad \langle \ln R_{30} \rangle = 4.65657. \tag{4.34}$$

So while there is no actual resistance at the value of the effective resistance in the system, it is still the result obtained by the model. This is due to the fact that the distribution is symmetric and therefore its mean value will be at the middle of the range. This translates to the fact that the current is equally likely to flow through the resistors with high and low resistance, with the total resistance been given by which resistance the current mainly flowed through in the network. This also explains why the peaks are moving closer together at higher values of n, as with a larger n value the greater the chance that the current will flow through an equal number of both high and low resistance areas, meaning that it will have an effective resistance closer to the value given by Dykhne's theorem.

The values for the natural log of the effective resistance of the systems and

that predicted by Dykhne are similar, the difference being given by

$$\Delta_{10} = \ln R_{\text{theo}} - \langle \ln R_{10} \rangle = 0.83053 \tag{4.35}$$

$$\Delta_{30} = \ln R_{\text{theo}} - \langle \ln R_{30} \rangle = 0.34343, \tag{4.36}$$

which is in line with with what is expected.

The standard deviation, σ, for this system is the distance the peaks are from the mean resistance. This is due to the distribution been made of two delta functions. But it can be seen that the standard deviation is smaller for a larger value of n, as

$$\sigma_{10} = 2.80673 \qquad \sigma_{30} = 1.76985. \tag{4.37}$$

Therefore the higher the value for n the closer the distribution peaks will get to the mean value and turning into a Gaussian distribution. This behaviour of σ is shown in fig.4.8. It can be seen that the relationship between the standard deviation and n goes as a slight curve before becoming almost linear around the value of $\sigma = 2$. From this it is seen that the peaks in the distribution will indeed get closer to the mean value. But as n increases the standard deviation will decrease more slowly and therefore the system will never actually reach a value of n where the two peaks will meet.

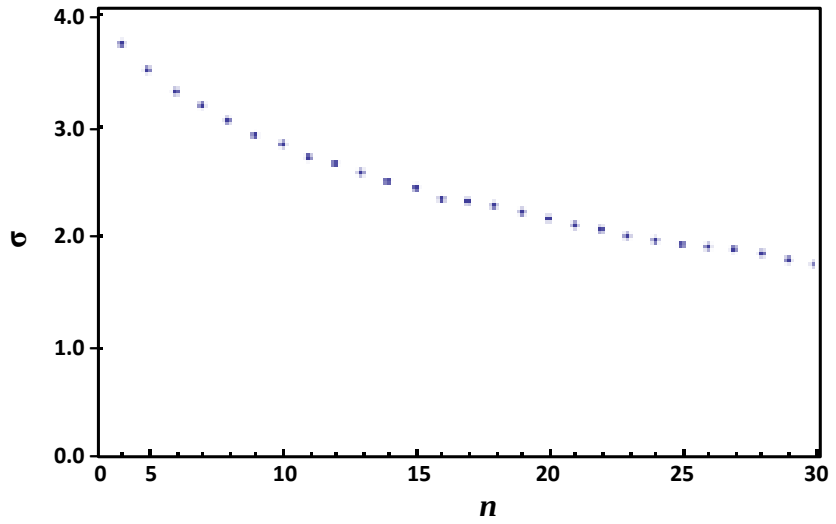

Figure 4.8: How the standard deviation changes with the changing size of the $n \times n$ matrices with a value of $\ln R_{\text{max}} = 10$, running over 1000 iterations.

The standard deviations relationship to $\ln R_{\text{max}}$ is given in fig.4.9. It can be seen that for small values of $\ln R_{\text{max}}$, the standard deviation has a curving be-

haviour but above the value of $\ln R_{\max} \approx 5$ this becomes a linear relationship. So when $\ln R_{\max} < 5$ the distribution will be seen to be similar to that of the normal distribution, looked at in section 4.2.1. This is due to the fact that the range of values for $\ln R$ is so small it is not possible to distinguish between the two peaks. Above $\ln R_{\max} = 5$ it is seen that the distribution is shown by the linear relationship.

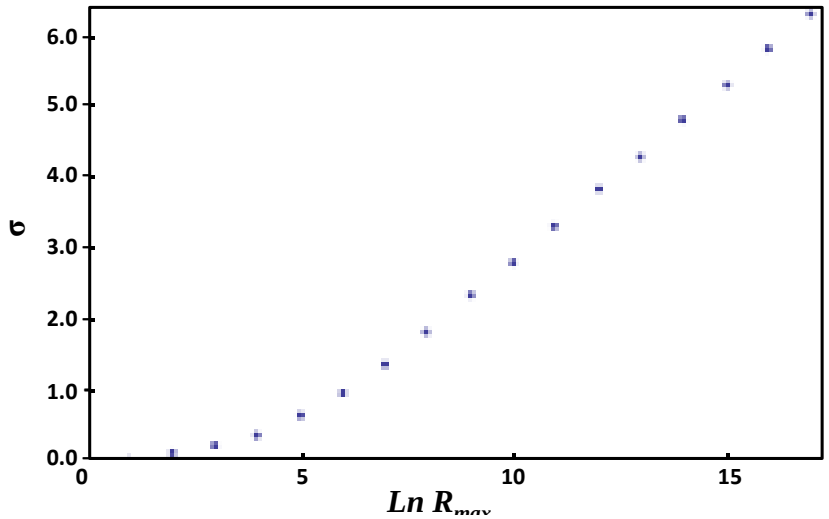

Figure 4.9: How the standard deviation changes with the changing value of $\ln R_{\max}$ for a 10×10 matrix, running over 1000 iterations.

From the analysis of this system it can be extrapolated that Dykhne's theorem can be used for all symmetric systems, even when there is no resistance at the value of the effective resistance predicted. As such it can be concluded that this theorem holds for all symmetric systems, and that using the transfer-matrix approach is a feasible way of producing the network of resistors that it can be applied too. Therefore this approach can now be applied to asymmetric systems to see if Dykhne's theorem will hold true for them also.

4.2.3 System with an Increasing Asymmetric Probability Distribution

This system is different from those previously looked at as the probability function used to define it is not a symmetric one. Instead it is a linearly increasing relationship, as shown in fig. 4.10a. Therefore the different values of resistance have different probabilities. This means that the network is made up of both open and closed resistors, and due to its asymmetric nature there are more open resistors than closed. Because of this, this system should have a similar distribution to the

one with the equal probability but it will have its mean value shifted and have a negative skew. This distribution is shown in fig. 4.10b. The skew is due to the fact that resistors with the higher values of resistance have a higher probability of being those which the current is travelling through. The value for the skewness, γ, of the system is

$$\gamma_{10} = -0.20546 \qquad \gamma_{30} = -0.01349. \tag{4.38}$$

The value of the effective theoretical mean can be calculated using Dykhne's theorem. But rather than using (4.4), the weighted mean for the model is used. This gives the equation for the effective resistance to be

$$\ln R_{\text{theo}} = \int_0^{\ln R_{\max}} \frac{2 \ln R}{(\ln R_{\max})^2} \ln R \, d \ln R = \frac{2}{3} \ln R_{\max} \tag{4.39}$$

for this probability distribution. Therefore (4.26) now becomes

$$\frac{2}{3} \ln R_{\max} = \langle \ln R \rangle \, . \tag{4.40}$$

This distribution has effective values of

$$\langle \ln R_{10} \rangle = 6.87968 \qquad \langle \ln R_{30} \rangle = 6.89247 \tag{4.41}$$

and from (4.39) the value from Dykhne's theorem is

$$\frac{3 \ln R_{\max}}{2} = 6.66666. \tag{4.42}$$

This gives a difference of

$$\Delta_{10} = \ln R_{\text{theo}} - \langle \ln R_{10} \rangle = 0.21302 \tag{4.43}$$

$$\Delta_{30} = \ln R_{\text{theo}} - \langle \ln R_{30} \rangle = 0.22587. \tag{4.44}$$

and the standard deviation for these two systems are

$$\sigma_{10} = 0.28399 \qquad \sigma_{30} = 0.09297. \tag{4.45}$$

From these values it can be seen that the difference for the 10×10 matrix is within a standard deviation of the expected value. But the difference for the 30×30 matrix is not. The value is rather $2.43\sigma_{30}$ away from the theoretical one. The values of the effective means themselves though, change very little with the size of the matrix. This is corroborated with data obtained by running the simulation for other values

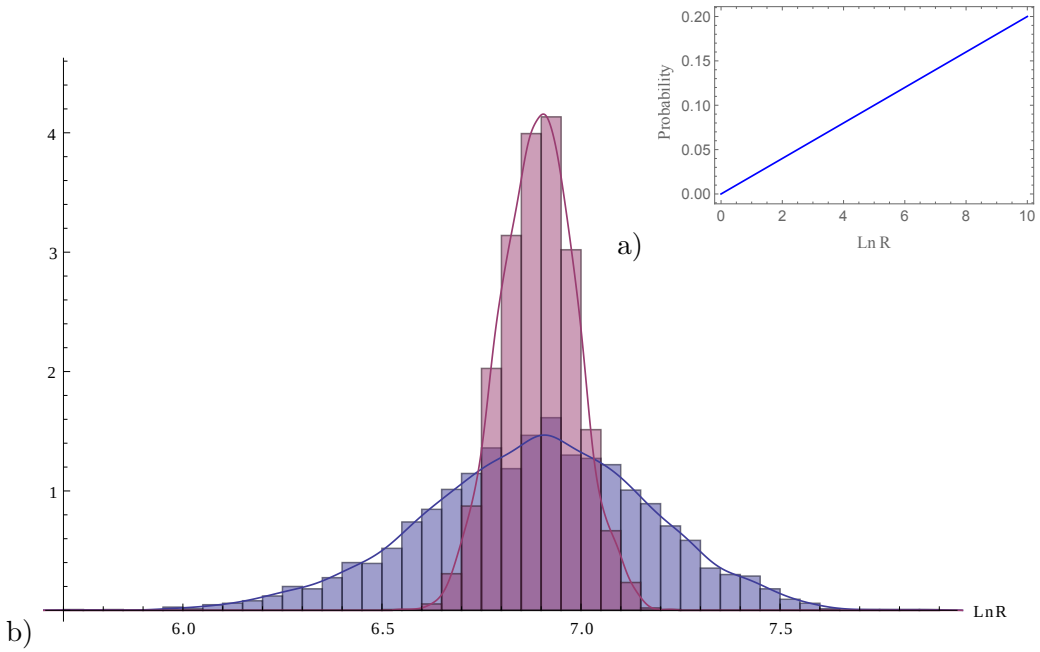

Figure 4.10: a) The increasing asymmetric probability. b) The distribution of the values of $\ln R$ for a range of $[0, 10]$. The blue shows the distribution for a 10×10 matrix and red for a 30×30 matrix, running over 3000 iterations.

of n, which gives the effective mean $\langle \ln R \rangle$, difference Δ, and the standard deviation σ to be

$$\begin{aligned} \langle \ln R_{50} \rangle &= 6.88876 & \Delta_{50} &= 0.22231 & \sigma_{50} &= 0.05436 \\ \langle \ln R_{40} \rangle &= 6.89135 & \Delta_{40} &= 0.22468 & \sigma_{40} &= 0.06669 \\ \langle \ln R_{20} \rangle &= 6.88107 & \Delta_{20} &= 0.21739 & \sigma_{20} &= 0.13917 \\ \langle \ln R_{5} \rangle &= 6.87264 & \Delta_{5} &= 0.20497 & \sigma_{5} &= 0.59355. \end{aligned} \tag{4.46}$$

Therefore from this, it can be extrapolated that for smaller values of n the effective mean given is less precise due to its higher value of σ, while conversely the larger matrices have a greater precision. But the actual values of the effective mean given for all the matrices looked at above, have a high accuracy. This is due to the fact that they are very similar, all being around $6.8 - 6.9$ when taken to two significant figures. As such the difference from the theoretical value is minimal, and varys little no matter what the size of the system. Therefore it can be assumed that these values are within a good alignment with that theorised by Dkyhne's theorem [34].

If the standard deviations, σ from (4.45) and (4.46) are plotted, with additional points, the decrease is clearer to see. This agrees with the above statement that the larger the network of resistors, the more precise the results become. This is shown in fig.4.11 where is can seen that when n is small the standard deviation decreases rapidly. It then slows until the point where at $n \approx 25$ the change in the value becomes negligible. Which is the same behaviour as that by the symmetric top hat probability distribution shown in section 4.2.1. This is expected considering both are linear distributions.

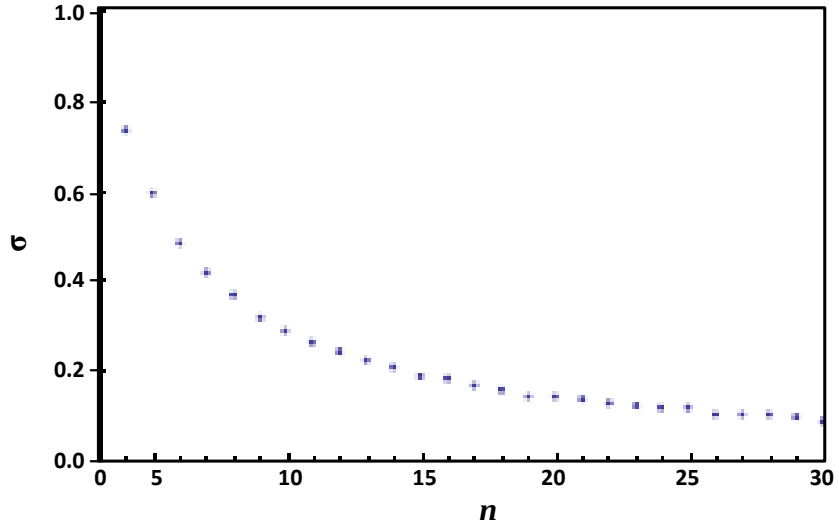

Figure 4.11: How the standard deviation, σ, changes with the changing size of the $n \times n$ matrices over a range of values for $\ln R = [0, 10]$, over 1000 iterations.

The last relationship to look at is the one between the standard deviation and the value of $\ln R_{\max}$. From Fig. 4.12 it can be seen that it is not quite linear, therefore for the lower values of $\ln R_{\max}$ the standard deviation varies less than for the higher values. Again similar in behaviour as that for the top hat distribution.

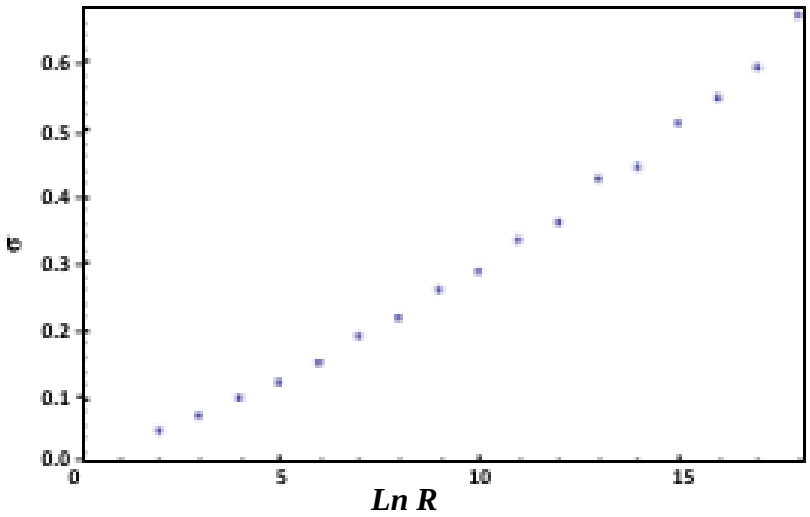

Figure 4.12: How the standard deviation, σ, changes with values of $\ln R_{\max}$ for a 10×10 matrix, running over 1000 iterations.

From this analysis it can be assumed that Dkyhne's theorem does indeed hold for this type of increasing asymmetric probability distribution. Further to that the behaviour of the system will be similar in nature to that of the symmetric top hat distribution.

4.2.4 System with a Decreasing Asymmetric Probability Distribution

The next asymmetric system looked into is that of a linearly decreasing probability, [fig. 4.13a]. Therefore this is a system with more closed resistors than open, as the probability of having a resistor with a low resistance is higher.

This system should again have a similar distribution to that of the symmetric case but it will have a positive skew. This is due to the current having a higher probability of travelling through the resistors with the lower resistance. The value of the skewness, γ is

$$\gamma_{10} = 0.25945 \qquad \gamma_{30} = 0.05903. \tag{4.47}$$

The theoretical effective mean for this distribution will again be given by the weighted mean. Therefore the equation for the effective resistance now becomes

$$\ln R_{\text{theo}} = \int_0^{\ln R_{\max}} \frac{2}{(\ln R_{\max})} \left(1 - \frac{\ln R}{\ln R_{\max}}\right) \ln R \, d \ln R = \frac{\ln R_{\max}}{3} \tag{4.48}$$

for this probability distribution. As such (4.26) now becomes

$$\frac{\ln R_{\max}}{3} = \langle \ln R \rangle \,. \tag{4.49}$$

The distribution, which is shown in fig.4.13b, has effective values for $\langle \ln R \rangle$ of

$$\langle \ln R_{10} \rangle = 3.09528 \qquad \langle \ln R_{30} \rangle = 3.1097 \tag{4.50}$$

and from Dykhne's theorem (4.49) for this system, becomes

$$\frac{\ln R_{\max}}{3} = 3.33333. \tag{4.51}$$

Therefore (4.50) varies from (4.51) by

$$\Delta_{10} = \ln R_{\text{theo}} - \langle \ln R_{10} \rangle = 0.23805 \tag{4.52}$$

$$\Delta_{30} = \ln R_{\text{theo}} - \langle \ln R_{30} \rangle = 0.22363. \tag{4.53}$$

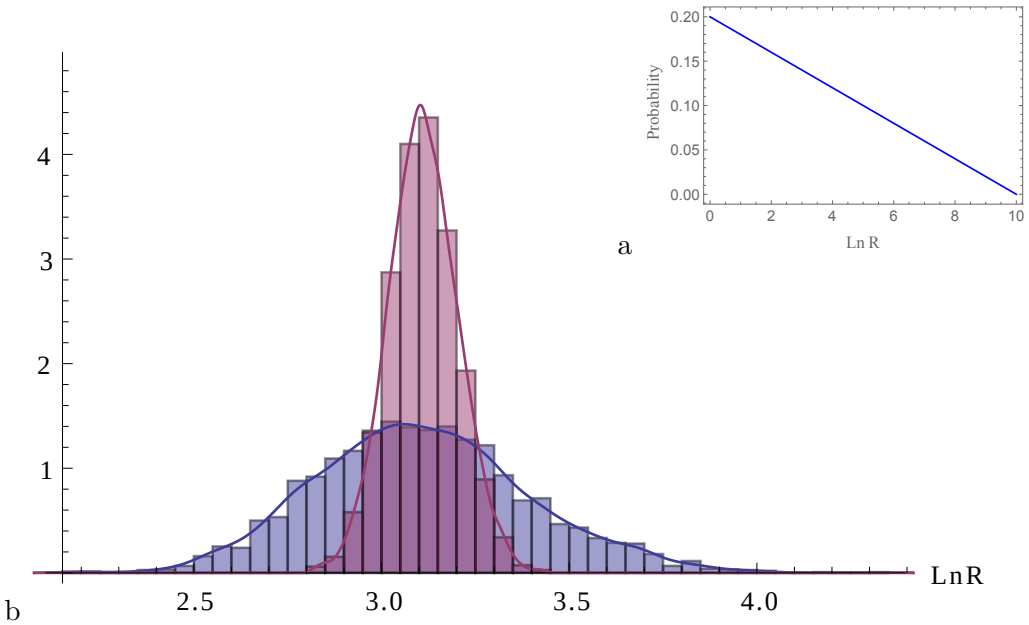

Figure 4.13: a) The decreasing asymmetric probability. b) The distribution of the values of $\ln R$ for a range of $[0, 10]$. The blue shows the distribution for a 10×10 matrix and red for a 30×30 matrix, running over 3000 iterations.

The standard deviation, σ, for this system is

$$\sigma_{10} = 0.28256 \qquad \sigma_{30} = 0.09159 \tag{4.54}$$

which shows that the effective mean for the 10×10 matrix is within a standard deviation of the mean given by Dykhne's theorem. Whereas the larger 30×30 matrix effective mean is $2.44\sigma_{30}$ away from from the theorised value. This is the same behaviour as seen in the asymmetric distribution shown in the previous section. Therefore it is expected that the extra data obtained from running the simulation for other values of n will have the same trends as that for the asymmetric linearly increasing probability. The values given in (4.55) shows that this is indeed true.

$$\begin{aligned}
\langle \ln R_{50} \rangle &= 3.10799 & \Delta_{50} &= 0.22534 & \sigma_{50} &= 0.05384 \\
\langle \ln R_{40} \rangle &= 3.10810 & \Delta_{40} &= 0.22523 & \sigma_{40} &= 0.06742 \\
\langle \ln R_{20} \rangle &= 3.10901 & \Delta_{20} &= 0.22433 & \sigma_{20} &= 0.13481 \\
\langle \ln R_{5} \rangle &= 3.04901 & \Delta_{5} &= 0.28433 & \sigma_{5} &= 0.60262.
\end{aligned} \tag{4.55}$$

From this, it can be seen that while the standard deviation decreases for the larger matrices, the values of the effective mean does not vary a great deal, concentrating around 3.1. And consequently the difference do not change excessive either. Therefore from this it can be extrapolated that while the values may be less precise, the accuracy of the result is the same for all the matrices [34]. As such it can be assumed that Dykhne's theorem does indeed give a good approximation for this network of resistors.

Plotting the values of the standard deviation σ given in (4.54) and (4.55) as well as further points, the decreasing behaviour can be seen clearly. This is shown in fig. 4.14, where the relationship between n the standard deviation σ can be seen to decrease rapidly with a curving behaviour. Again this behaviour is similar to that shown for the symmetric top hat distribution in section 4.2.1 and that shown the the increasing asymmetric distribution in section 4.2.3. Which is expected. Now to look at how the standard deviation changes with different values of $\ln R_{\max}$. From fig. 4.15 it can be seen that it is not quite linear and the standard deviation varies less at the lower values of $\ln R_{\max}$. Again similar to the previous two linear distributions.

This analysis shows that Dykhne's theorem holds as a good approximation for this linear asymmetric distribution at small values of n as well, whereas at larger matrices the value will still have the same accuracy, but that the precision of the measurements will not be so great.

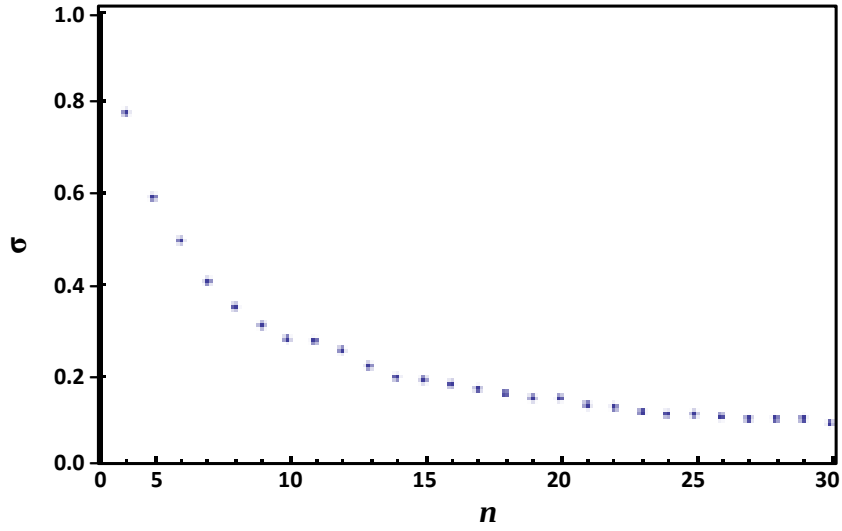

Figure 4.14: How the standard deviation, σ, changes with the changing size of the $n \times n$ matrices with a range of values being $\ln R = [0, 10]$, over 1000 iterations.

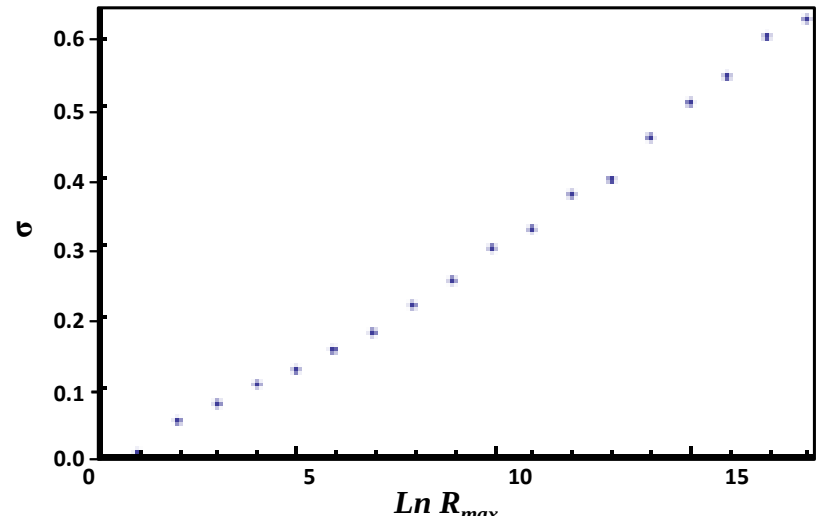

Figure 4.15: How the standard deviation, σ, changes with increasing values of $\ln R_{\max}$ for a 10×10 matrix, running over 1000 iterations.

4.3 Conclusion

From the analysis given in the previous sections in this chapter, it can be extrapolated that the assumption stated in Chapter 3 is an appropriate one to use. This is due to the fact that the distribution stated in that model which includes tunnelling, shown in fig.4.1, is one which is made up of a combination of the top hat potential

and linear asymmetric ones. It has been shown that for both the symmetric and asymmetric parts of this distribution, the theoretical value will hold. That even when the precision of the assumption is less, the accuracy will remain the same. As such using Dykhne's theorem as a way to calculate the mean of the varying potentials including tunnelling is an good approximation to make.

Chapter 5

Edge States

The edge states of the system are an important contribution to the current and thermopower in the Hall bar geometry, one which is not taken account of in the model in chapter 3. As such a way to include them into this model is needed, thus making a more complete picture. This picture can then be compared to the experimental data for the thermopower presented in [3], and explained in chapter 2.

The first thing that needs to be done, is to look at how the current moves around the system in the bar geometry. Fig.5.1 shows how the current travels through the bulk of the system from the hot region to the colder one, which is expected. At the edges though the current runs in opposite directions. This is due to the potential difference at the end nodes which connect the two sides and drives the current to travel in a clockwise direction around the system. This difference in directions produces different chemical potentials in each edge [2]. So from fig.5.1 it can be seen that the chemical potential on the left-hand edge will be given by the hot node, μ_1. Therefore the particles which are carrying the left-hand channel's current, will fill up to that state. The right-hand side conversely will be given by chemical potential from the cold node, μ_2, due to the current being driven from that node to the hot one.

Now the movement of the current through the material in the bar geometry has been described, The next thing to consider is how the Landau levels behave at the edges. As stated in 1.2, the quantum Hall effect appears in an incompressible fluid, and when the edges are included it becomes defined in a finite potential well. As such when the Landau levels reach those edges, which act as the walls of the well, they bend up. This means that the edge states can be filled above the Fermi level of the bulk [2]. This is shown in fig. 5.2.

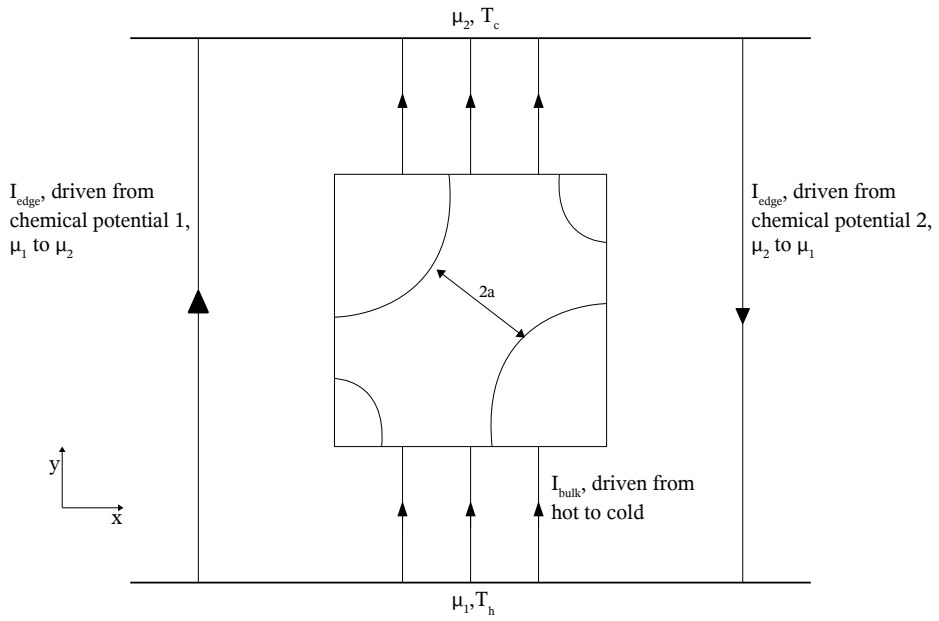

Figure 5.1: A sketch to show how the current will travel through the system which consists of both the bulk and the edges. This shows where the chemical potential difference is coming from int he system.

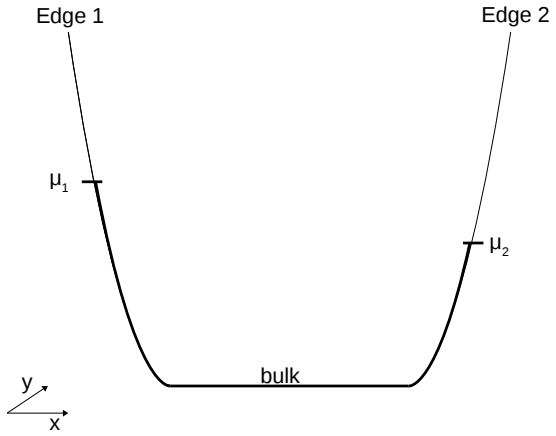

Figure 5.2: A cross-section of the bar showing how the Landau level states are filled up to the chemical potentials in both edges. The current through the bulk is going into the page.

From this it can be seen that rather the distinct regions of localization that appear in the bulk of the material [14], the particles moving along the edges do so in quasi-one-dimensional states. These states appear all the way up to the chemical potential [31]. As such the equation which describes this behaviour for the system

being investigated in this thesis can be derived from the current equation

$$I = Anve, \tag{5.1}$$

where A is the cross-sectional area, n is the number density, v is the drift velocity, and e is the charge of the particles [35]. How this is used is shown in depth the next section.

5.1 Current Derivation

Using the general current equation (5.1) to derive the current for the edges states in the quantum Hall bar geometry, it must first be defined that the cross-sectional area, $A = 1$. This is due to the fact that the edges states are being treated as quasi-one-dimensional. Therefore the only parts of (5.1) that will contribute are the drift velocity of the eigenstates on the edge, v, the number density of the current, n and e, which is the charge of an electron. The equations for v and n are given by [36]in k-space condensed matter physics which take the form

$$v = \frac{1}{\hbar}\frac{\partial \epsilon}{\partial k}, \tag{5.2}$$

$$n = g(\epsilon)f(\epsilon), \tag{5.3}$$

where $g(\epsilon)$ is the density of states and $f(\epsilon)$ is the probably of the particle being in each state. For the system being investigated, $f(\epsilon) = f(\epsilon - \mu, T)$ is given by the Fermi-Dirac distribution. When this information is put into (5.1), then it becomes

$$I = \frac{1}{\hbar}\frac{\partial \epsilon}{\partial k}\, e\, g(\epsilon) f(\epsilon - \mu, T), \tag{5.4}$$

which is the generalised starting point to derive the edge current for this system. The next step is to convert the density of states from its energy dependence, to a spacial one, $g(\vec{k})$. This is done using the relation that

$$g(\epsilon) = 2g(\vec{k})\frac{dk}{d\epsilon} \tag{5.5}$$

in (5.4). This now gives the current to be given by

$$I = \frac{e}{\hbar} 2g(\vec{k}) f(\epsilon - \mu, T). \tag{5.6}$$

The equation that defines $g(\vec{k})$ in the 2-dimensions for a single point [11] is

$$g(k) = \frac{1}{(2\pi)^2} d^2\vec{k}. \tag{5.7}$$

The reason to look at the density of sates in 2-dimensions is because when the plateaus form the particles moving in the material become a 2-dimensional electron gas, as I stated in chapter 1.

Therefore to find the density of states for the whole system, which is that which is required for the number density, then the whole system will need to be summed over. This gives

$$n = \sum \frac{1}{(2\pi)^2} d^2\vec{k}\, f(\epsilon - \mu, T), \tag{5.8}$$

which when taken to the infinite limit, the sum becomes an integral. As such (5.8) becomes

$$n = \int \frac{1}{(2\pi)^2} f(\epsilon - \mu, T)\, d^2\vec{k}. \tag{5.9}$$

Now the Fermi-Dirac function for $f(\epsilon - \mu, T)$ needs to included into the equation for the number density n. This is given by

$$f(\epsilon - \mu, T) = \frac{1}{\exp((\epsilon - \mu)/k_B T) + 1} \tag{5.10}$$

which, when mapped to the regime where the temperature is measured in energy units, becomes

$$f(\epsilon - \mu, T) = \frac{1}{\exp((\epsilon - \mu)/T) + 1}. \tag{5.11}$$

Adding (5.11) into (5.9) the equation for the number density is now given by

$$n = \frac{1}{(2\pi)^2} \int \frac{1}{\exp((\epsilon - \mu)/T) + 1}\, d^2\vec{k'}. \tag{5.12}$$

The next stage of the current deviation involves converting the integral from the spacial regime, to the energy one. To achieve this, the integral must first be transferred from Cartesian co-ordinates, which are given by $d^2\vec{k} = dk_x dk_y$, to Polar ones, such that

$$d^2\vec{k} = 2\pi k\, dk. \tag{5.13}$$

Then taking the relationship that

$$\epsilon = k^2, \tag{5.14}$$

and differentiating with respect to k, it will become

$$d\epsilon = 2k\, dk. \tag{5.15}$$

As such putting this into (5.13), the replacement variable that the integral will be calculated over becomes

$$d^2\vec{k} = \pi\, d\epsilon. \tag{5.16}$$

So now putting this into (5.17) we get

$$\begin{aligned} n &= \frac{1}{(2\pi)^2} \int \frac{1}{\exp((\epsilon-\mu)/T)+1}\, \pi\, d\epsilon \\ &= \frac{1}{4\pi} \int \frac{1}{\exp((\epsilon-\mu)/T)+1}\, d\epsilon. \end{aligned} \tag{5.17}$$

Therefore the equation for deriving the current (5.6) is given by

$$\begin{aligned} I &= \frac{2e}{\hbar}\frac{1}{4\pi} \int_0^\infty \frac{1}{\exp((\epsilon-\mu)/T)+1} d\epsilon \\ &= \frac{e}{2\hbar\pi} \int_0^\infty \frac{1}{\exp((\epsilon-\mu)/T)+1} d\epsilon. \end{aligned} \tag{5.18}$$

Doing this integral gives the edge current to be

$$I_{\text{edge}} = \frac{e}{2\pi\hbar} T \ln\left(1+\exp\left(\frac{\mu}{T}\right)\right). \tag{5.19}$$

Now using this solution it is possible to derive the conductivity of the the edges states, both thermal and electrical. From these conductivity's the equation for the thermopower through the edges states can be found.

5.2 Thermal Conductance

The thermal conductance, σ_{th}, of the edge states is given by the equation

$$\sigma_{\text{th}} = \frac{\partial I_{\text{edge}}}{\partial \Delta T}. \tag{5.20}$$

where I_{edge} is the heat current for the particles in the edges and gives their movement due to the temperature gradient, which is given by ΔT, and from here onwards will be notated as T [37]. Therefore by differentiating (5.19) by T the thermal

conductance becomes

$$\begin{aligned}\sigma_{\text{th}} &= \frac{\partial}{\partial T}\left(\frac{e}{2\pi\hbar}T\ln\left(1+\exp\left(\frac{\mu}{T}\right)\right)\right) \\ &= -\frac{e\,\exp\left(\frac{\mu}{T}\right)\mu}{2T\left(1+\exp\left(\frac{\mu}{T}\right)\right)\hbar\pi} + \frac{e\,\ln\left(1+\exp\left(\frac{\mu}{T}\right)\right)}{2\pi\hbar}.\end{aligned} \tag{5.21}$$

This equation can be further simplified by using the relationship that $h = 2\pi\hbar$ and the law of exponentials that $\exp(A)\exp(-A) = 1$. Therefore (5.21) will now become

$$\sigma_{\text{th}} = \frac{e}{h}\left(\ln\left(1+\exp\left(\frac{\mu}{T}\right)\right) - \frac{\mu}{T\left(1+\exp\left(-\frac{\mu}{T}\right)\right)}\right). \tag{5.22}$$

5.3 Electrical Conductance

The electrical conductance, σ_{el}, is found in a similar way to the thermal. It is also a differential equation which is given by

$$\sigma_{\text{el}} = \frac{\partial I_{\text{edge}}}{\partial \Delta V}. \tag{5.23}$$

But it can bee seen that (5.19) does not contain a direct relationship between the current, I_{edge}, and the voltage difference, ΔV, which for future ease will be referred to as V. But it does contain the chemical potential μ, which is related to the voltage by

$$\mu = -\frac{eV}{2}. \tag{5.24}$$

Therefore if (5.23) is rewritten using the differential chain rule it will become

$$\sigma_{\text{el}} = \frac{\partial I_{\text{edge}}}{\partial \mu}\frac{\partial \mu}{\partial V}, \tag{5.25}$$

where $\frac{\partial \mu}{\partial V} = -e/2$ from (5.24). As such (5.25) is now

$$\sigma_{\text{el}} = -\frac{e}{2}\frac{\partial I_{\text{edge}}}{\partial \mu}. \tag{5.26}$$

Applying this equation to (5.19) then the electrical conductance becomes

$$\begin{aligned}\sigma_{\text{el}} &= -\frac{e}{2}\frac{\partial}{\partial \mu}\left(\frac{e}{2\pi\hbar}T\ln\left(1+\exp\left(\frac{\mu}{T}\right)\right)\right) \\ &= -\frac{e^2\exp\left(\frac{\mu}{T}\right)}{4\left(1+\exp\left(\frac{\mu}{T}\right)\right)\hbar\pi}.\end{aligned} \tag{5.27}$$

This can be simplified once more by using the relations of $h = 2\pi\hbar$ and $\exp(A)\exp(-A) = 1$. As such (5.27) becomes

$$\sigma_{\text{el}} = -\frac{e^2}{2h\left(1+\exp\left(-\frac{\mu}{T}\right)\right)}. \tag{5.28}$$

5.4 Thermopower

The equation that defines the thermopower in general is

$$S_{xx} = -\frac{\Delta V}{\Delta T}, \tag{5.29}$$

which can be taken to the limit where the Δ's become differential's such that S_{xx} is now defined as

$$S_{xx} = -\frac{\partial V}{\partial T}. \tag{5.30}$$

Using the chain rule this can be rewritten for the edges as

$$S_{edge} = -\frac{\partial V}{\partial I_{\text{edge}}}\frac{\partial I_{\text{edge}}}{\partial T} \tag{5.31}$$

which in turn can be expressed using (5.20) and (5.23) such that

$$S_{\text{edge}} = -\frac{\sigma_{\text{th}}}{\sigma_{\text{el}}}. \tag{5.32}$$

This holds true for the thermopower in a general situation and not just at the one looked at in this thesis [[38], [39]]. So using(5.22) and (5.28) and the equation for the thermopower for the edge states of this model is

$$\begin{aligned} S_{\text{edge}} &= \frac{\frac{e}{h}\left(\ln\left(1+\exp\left(\frac{\mu}{T}\right)\right) - \frac{\mu}{T\left(1+\exp\left(-\frac{\mu}{T}\right)\right)}\right)}{-\frac{e^2}{2h\left(1+\exp\left(-\frac{\mu}{T}\right)\right)}} \\ &= \frac{\ln\left(1+\exp\left(\frac{\mu}{T}\right)\right) - \frac{\mu}{T\left(1+\exp\left(-\frac{\mu}{T}\right)\right)}}{\frac{-e}{2\left(1+\exp\left(\frac{-\mu}{T}\right)\right)}} \\ &= -\frac{2\left(\exp\left(-\frac{\mu}{T}\right)+1\right)\ln\left(1+\exp\left(\frac{\mu}{T}\right)\right) - 2\frac{\mu}{T}}{e}. \end{aligned} \tag{5.33}$$

5.5 Defining the Chemical Potential

The main variable in equation (5.33) is the chemical potential, μ. Therefore a way to define this is required before this equation can be used in the model which represents the thermopower of the system. This definition must also be in line with the equations for the energy gaps given in the original model for the bulk material, explained in chapter 3. The first thing that must be investigated therefore, is how the chemical potential interacts with the disorder created by the screening in the bulk region of the material. Once that has been established, the behaviour and interaction of the μ and the Landau levels can be derived. This will thus lead to a definition of how the chemical potential contributes to the current and the thermopower of the system.

5.5.1 Derivation of the Chemical Potential

Looking back at fig. 5.1 and fig. 5.2 (which are both reproduced in 5.3) then it can be seen that the chemical potential of the two edges of the Hall bar are different. This is due to the way the particles are moving around the system. It is this difference which gives rise to the contribution from the edges states to the total current and thermopower.

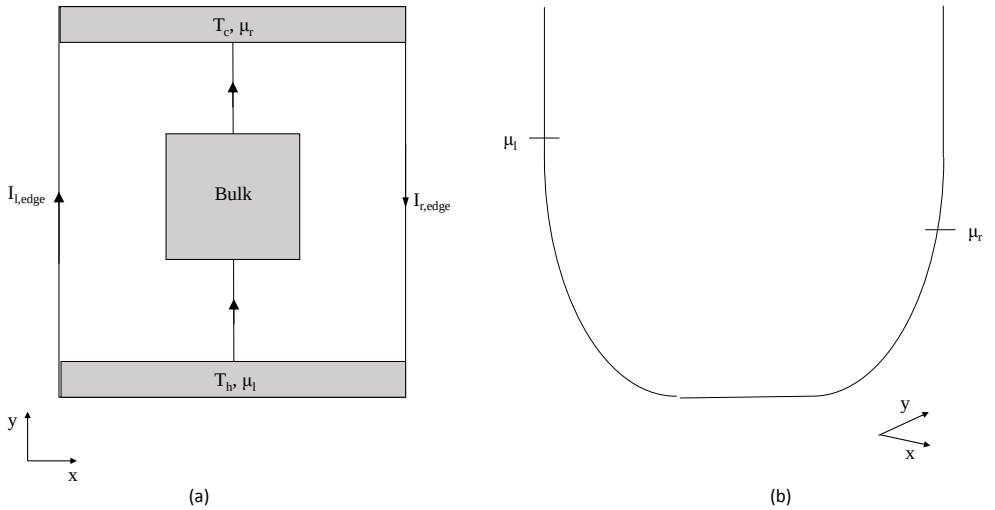

Figure 5.3: (a) A sketch showing how the particles move around the edges in the Hall system. (b) A cross-section of system showing how the chemical potentials are different on the edges.

From fig.5.3(b) the two chemical potentials, shown as μ_l, and μ_r, are different. But as the magnetic field varies, then so will the position of the chemical potential in the Landau level. Therefore the value, and the relationship between the two edge chemical potentials, will be dependent on where along the plateau the measurement is taking place. To find out how this variation should be expressed it is useful to first look at the situation where the Fermi level is sitting at the centre of the plateau. At this position the chemical potential on the edges hold the same value due to the fact that at this position the only contribution is from the bulk of the material. Therefore it can be written that

$$|\mu_l| = |\mu_r| = \frac{\Delta}{2}. \tag{5.34}$$

Then using the assumption given in [6] that

$$\mu_l = -\mu_r \tag{5.35}$$

an equation that relates μ_i to the plateau width and the position on the plateau that the particles are, can be derived. If this was a perfect system without any disorder, then the chemical potential would stay at a constant value of $\Delta/2$. But this isn't a perfect system, and it does contain disorder, the saddle points from the screening potential in the bulk being the main contributions to this. Therefore the value of the chemical potential will change as we move across the plateau. How this change is affected by the disorder is shown in fig. 5.4.

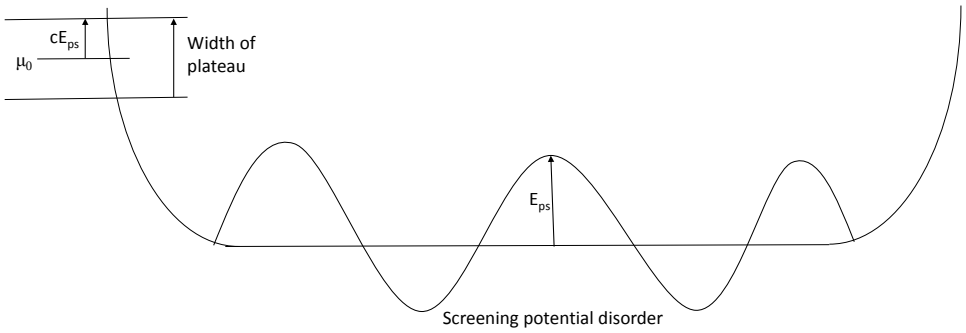

Figure 5.4: A sketch showing how the chemical potential fluctuates with the screening potential. $\mu_0 = \Delta/2$, and c is the variable that relates the saddle point heights E_{sp} with is the amount the chemical potential fluctuates from its $\Delta/2$ position.

Using fig. 5.4 it can see that the variation in μ is dependant on the height of the saddle point, E_{sp}. This in turn is dependant upon where on the plateau the

particle is sitting, g, which is the ratio of the position of the particle on the plateau with its width, $g = \delta\nu/\delta\nu_m$. As such it ranges between [-1,1] no matter the size of the plateau, and holds the value of zero in the centre. This was described in more detail in chapter 3. A such the equation for μ can be written as

$$\mu = \mu_0 + E_{ps}c, \tag{5.36}$$

where c is a transitional constant that will be discussed in section 5.5.2. This becomes, when $\mu_0 = \Delta/2$ and $E_{ps} = (1-g)\Delta/2$ are substituted in, becomes

$$\mu = \frac{\Delta}{2} + (1-g)\frac{\Delta}{2}c. \tag{5.37}$$

If this is looked at in the position where $g = 0$, which is the centre of the plateau, then μ should equal $\Delta/2$ as defined above. But currently it does not. Therefore the equation is not yet complete. To correct (5.37), then a extra term must be added in such a form that it removes the remainder $\frac{\Delta}{2}c$ from μ_0. Therefore the equation for μ must become

$$\begin{aligned}\mu &= \frac{\Delta}{2} + (1-g)c\frac{\Delta}{2} - c\frac{\Delta}{2} \\ &= \frac{\Delta}{2} - cg\frac{\Delta}{2} \\ &= (1-cg)\frac{\Delta}{2}.\end{aligned} \tag{5.38}$$

This is the equation which will be used to define the chemical potential in the model being created.

5.5.2 The Transition Value

In equation (5.38) the notation c is used for the variable that relates the saddle point heights to the chemical potential. This variable determines how the chemical potential is going to be affected by the disorder of the system, and is known as the transition value. It can therefore also be described as the point where the chemical potential from the Landau level above will start to interact with the one in the equation due to its fluctuations. This is shown in fig. 5.5.

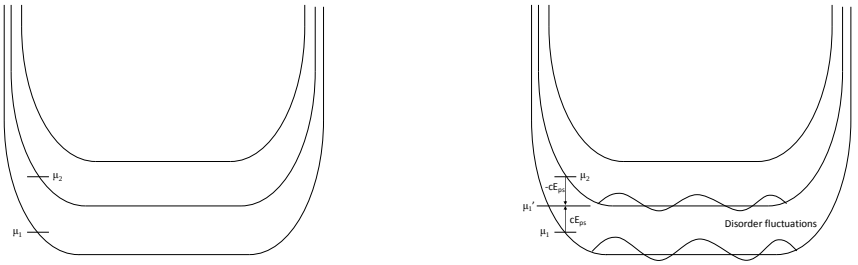

(a) Shows the basic lay out of the chemical potentials in a non-disordered system.

(b) Shows how the disorder can move μ_1 so that μ_2 interacts with it.

Figure 5.5: Sketches showing the different Landau levels and the chemical potentials and how the disorder creates the transition value c.

Fig. 5.5b show that if the variation in μ_1 due to the background potential is large enough, it will move within close proximity to μ_2, which will then affect its behaviour. This is the transition point of the edge states. This can been seen more clearly in fig. 5.6 where it is shown how the chemical potential moves off of the plateau before its end. This is the point where the higher chemical potential is starting to interact with the edge state being looked at.

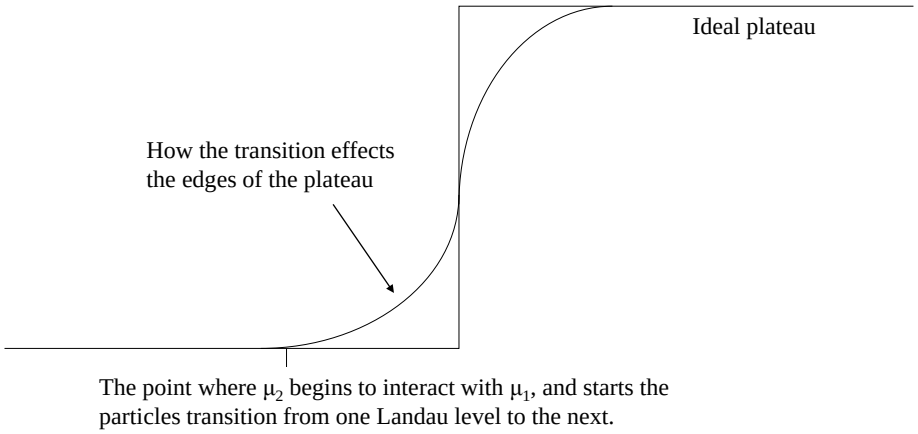

Figure 5.6: A stekch to show how the chemical potential from the higher Landau level affects the transition from the plateau of one quantum hall state to the next. It also shows how this interaction changes the size of the plateau itself, making it smaller than than the ideal plateau which will have no background potential interfering with the chemical potential.

From all of this it can be seen that the transition variable, c, is dependent

upon the width of the plateau. Now considering (5.38) gives that

$$\mu = (1 - cg)\frac{\Delta}{2}, \tag{5.39}$$

then to work out the range of values c could hold, what happens to the chemical potential in the limits of the saddle point energy values needs to be investigated. So if the screening potential is very weak, the value of E_{ps} is very small, then the chemical potential will vary very little from its central position. As such it will have little to no interaction with the chemical potential from the Landau level above. Whereas if E_{ps} is large then the variation in the chemical potential will also be large, and the interference from higher Landau levels will need to be taken into consideration. What this means is that when E_{ps} is weak, $\mu \approx \frac{\Delta}{2}$, and therefore $c = 0$. When E_ps is strong $\mu \approx (1 - g)\frac{\Delta}{2}$. This is due to the fluctuations being so strong that the chemical potential takes the same form as the disorder potential. Therefore the interaction with the other Landau levels will be great. As such in this case, $c = 1$. This argument gives the range of values for c to be [0,1].

To consider how to use the above information in the model, it must be assumed that the lower the temperature the higher the disorder is going to be within the system. This is because at lower temperatures tunnelling needs to be taken into account as well as the concept that the lower the temperature of the system, the greater effect the disorder screening potential will have upon the other energies involved, i.e the chemical potential. Therefore it is possible to derive an equation for c from all this data. It must be a ratio that does not exceed 1, that shows the relationship between the actual plateau and the width of one that contains no edge effects. This is due to the fact that the transition value contributes largely to the width of the plateau, making it smaller when the disorder is higher. But it also needs to be a larger number when the plateau width is at its smallest. The plateau widths in the equation will also not be the whole plateau. This is due to the fact that it is only half the plateau that is affected by the chemical potential in the Landau level above, as seen in fig. 5.6 and fig. 5.3. From all of this is can been seen that the equation needed to define this transition value is

$$c = \frac{1/B_{r,0} - 1/B_{r,max}}{1/B_{o,0} - 1/B_{o,max}}, \tag{5.40}$$

where $B_{r,i}$ are the values of the magnetic field of the plateau we are looking at and, $B_{o,i}$ are the magnetic field values of an plateau without edge effects. For both plateaus the values at the centre, 0, and the edge, max, are needed. A simpler way

of looking at this is considering the filling factor, ν in (5.40) due to the relation

$$\nu = \frac{nh}{eB}. \tag{5.41}$$

Using this (5.40) can be written such that

$$c = \frac{\nu_{r,0} - \nu_{r,max}}{\nu_{o,0} - \nu_{o,max}}, \tag{5.42}$$

which can be related to the electrical conductance σ_{el} via [4],

$$\sigma = \nu \frac{e^2}{h}, \tag{5.43}$$

therefore c can be written in terms of this parameter. And because the changes being looked at are given by the background potential, then the only conductance with relevance to c will be that given by the bulk. So (5.42) will now become

$$c = \frac{\sigma_{r,0} - \sigma_{r,max}}{\sigma_{o,0} - \sigma_{o,max}}. \tag{5.44}$$

This conductance can be easily obtained from the equation for the bulk thermopower which takes into account the tunnelling, given in chapter 3. Therefore the transition value for the edge states can be equated and incorporated into the model.

5.6 Edge Current

Now that the chemical potential μ has been defined, as well as the transition value c, the final component of the edge current, which will be part that comes from the contribution from the Landau level above must be incorporated into the equation. This is done by including a term that is dependant on the negative transition value, $-c$. Therefore the edge current will become

$$I_{\text{edge}} = I'_{\text{edge}}(\mu[c]) + I'_{\text{edge}}(\mu[-c]), \tag{5.45}$$

where

$$\mu[c] = (1 - gc)\Delta/2, \qquad \text{and} \qquad \mu[-c] = -(1 - gc)\Delta/2 \tag{5.46}$$

Therefore the equation which defines the current travelling through the edge of the system must be given by

$$I_{\text{edge}} = \frac{e}{2\pi\hbar} T \left(\ln \left(1 + \exp \left(\frac{\mu[c]}{T} \right) \right) + \ln \left(1 + \exp \left(\frac{\mu[-c]}{T} \right) \right) \right). \tag{5.47}$$

This is the equation that will be used in the model being constructed in this thesis.

Chapter 6

Simplistic Model

In chapter 5 and [6], the current that is travelling through the edges and bulk has been derived. Using these, it is possible to construct an equation that will express the total current running through the Hall bar system. Then using this, the thermopower for a simplistic - non-tunnelling, model can be derived. This is done in the next two sections, the first devoted to the assembling the total current of the system, and the second given other to the study of the thermopower.

6.1 Total Current Derivation

The total current of the system will be given by a combination of the edge current, and the bulk current. For the Hall effect, how these combine does not matter. The particular configuration of current does not change the results. But when investigating the thermopower, how they split plays a big part in the results. Therefore how they come together to make up the total net current, needs to be defined before the thermopower of the system can be derived. In fig.6.1 the two extremes, all the current contribution coming from the bulk [fig.6.1a] or all the current coming for the edges [fig.6.1b]are shown. But the true system is a combination of these two scenarios. Therefore when an equation is written down for the total, net current, I, of the system, it looks like

$$\begin{aligned} I &= I_{\text{edge contribution}} + I_{\text{bulk contribution}} \\ &= \alpha I_{\text{edge}} + (1-\alpha) I_{\text{bulk}}, \end{aligned} \tag{6.1}$$

where α is a parameter which defines the way the current splits. It ranges from [0,1]. This variable is called a free parameter, as there is no way to determine how much of the current is travelling through the bulk, and how much is going through

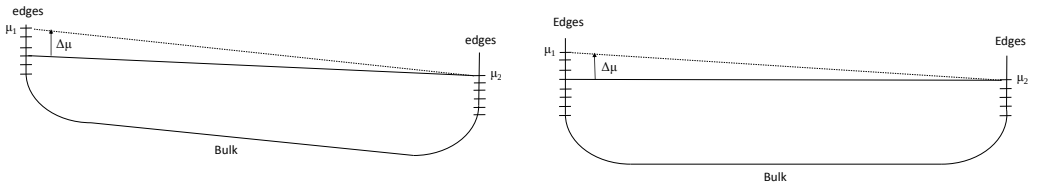

(a) Current travelling through the bulk only. (b) Current travelling through the edge only.

Figure 6.1: Sketches to show how the current will flow through the system in the extreme cases, looking at one Landau level. a) give the current contribution from the bulk only, this is due to the fact that while it is the different chemical potentials on the edges which gives the net difference $\Delta\mu$, the number of energy levels on both sides are the same. Therefore the difference is given up the variation in the bulk. b) gives current contribution from the edges only. It can clearly be seen here that there is a difference in the number of energy levels that are filled, and this is therefore where the chemical potential difference $\Delta\mu$ comes from.

the edges at any given time. Therefore when the model is being tested later, it will be run for a range of values for this parameter, to see which gives simulated results similar to that of the experimental data from [3].

Putting the current equation for the bulk (3.2), and the edges (5.47) into (6.1) will give the total net current for the system. This equation is

$$\begin{aligned} I =& \frac{e}{h}\Bigg(\alpha T\left(\ln\left(1+\exp\left(\frac{\mu[c]}{T}\right)\right)-\ln\left(1+\exp\left(\frac{\mu[-c]}{T}\right)\right)\right) \\ &+(1-\alpha)\left(-(qe)\delta V+\left(1+\frac{E_{sp}}{T}\right)\delta T\right)\exp\left(-\frac{E_{sp}}{T}\right) \\ &-(1-\alpha)\left((qe)\delta V+\left(1+\frac{E_{sh}}{T}\right)\delta T\right)\exp\left(-\frac{E_{sh}}{T}\right)\Bigg) \end{aligned} \tag{6.2}$$

and this will be used throughout the rest of this chapter to derive the thermopower of this non-tunnelling system.

6.2 Deriving The Thermopower

The thermopower of the system is given by

$$S_{xx} = -\frac{\Delta V}{\Delta T} \tag{6.3}$$

which, as has already been shown in fthe chapter 5, can also be derived using the ratio of the thermal and electrical conductances. Therefore the following sections will be devoted to formulating these equations for the model being created.

6.2.1 Thermal Conductance

The thermal conductance is given by the same equation given in chapter 5 (5.20). This equation is given by

$$\sigma_{\text{th}} = \frac{\partial I}{\partial \Delta T}, \tag{6.4}$$

but before this can be applied to the total current equation found in section 6.1, how the temperature gradient propagates across the material needs to be investigated. This is shown in fig.6.2

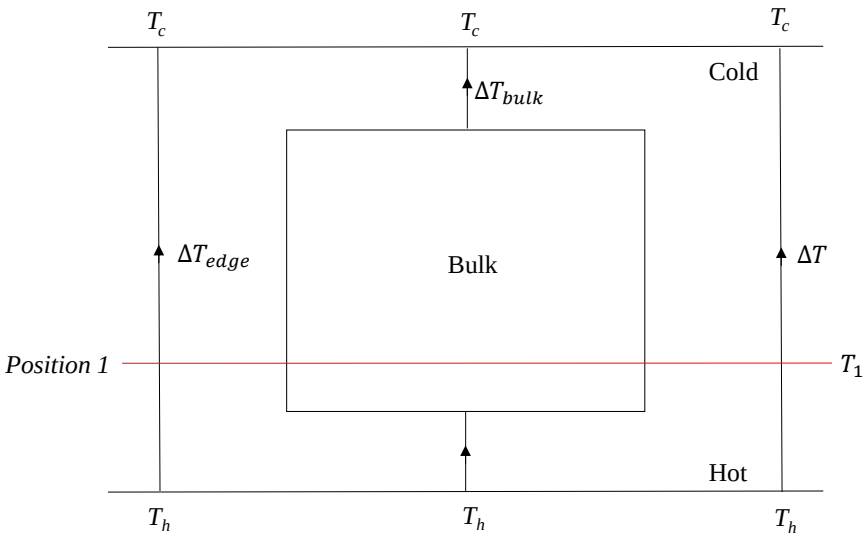

Figure 6.2: a sketch showing how the temperature gradient propagates through the material. Position 1 is a random place along the material. The red line shows how the temperature along that position is the same no matter if you are on the edge or the bulk.

From 6.2 it can be seen that at any point along the temperature gradient, the temperature in bulk is the same as that on the edges. This is an assumption that is made to simplify the model. It assumes that the temperature at the T_h node and the T_c node are constant. This is an acceptable assumption to make, because even if it is not true, the variation will be minimal in concern to other variables in the equation. Therefore it will not make any serious difference to the model being derived. From this assumption it can be written that $\Delta T = \alpha \Delta T_{\text{edge}} + (1-\alpha)\Delta T_{\text{bulk}}$

where, $\Delta T_{\text{edge}} = \Delta T_{\text{bulk}}$. Which will give the deviation variable in (6.4) to be just ΔT, and as such having no need to define if it applies to the bulk or the edge. in the derivation below, and further development of this model, the abbreviation that $\Delta T \to T$ will be used. Therefore equation (6.4) will now become

$$\begin{aligned}\sigma_{\text{th}} = \frac{1}{h}\frac{\partial}{\partial T}\Bigg(&\alpha e T\left(\ln\left(1+\exp\left(\frac{\mu[c]}{T}\right)\right)-\ln\left(1+\exp\left(\frac{\mu[-c]}{T}\right)\right)\right)\\&+(1-\alpha)\left(-(qe)\delta V+\left(1+\frac{E_{sp}}{T}\right)\delta T\right)\exp\left(-\frac{E_{sp}}{T}\right)\\&-(1-\alpha)\left((qe)\delta V+\left(1+\frac{E_{sh}}{T}\right)\delta T\right)\exp\left(-\frac{E_{sh}}{T}\right)\Bigg),\end{aligned} \tag{6.5}$$

which gives

$$\begin{aligned}\sigma_{\text{th}} = \frac{e}{h}\Bigg(&\alpha\left(-\frac{\mu[c]\,\exp\left(\mu[c]/T\right)}{T\left(1+\exp\left(\mu[c]/T\right)\right)}+\ln\left(1+\exp\left(\frac{\mu[c]}{T}\right)\right)\right)\\&-\alpha\left(\frac{\mu[-c]\,\exp\left(\mu[[-c]/T\right)}{T\left(1+\exp\left(\mu[-c]/T\right)\right)}+\ln\left(1+\exp\left(\frac{\mu[-c]}{T}\right)\right)\right)\Bigg)\\&+\frac{qe}{h}\left((1-\alpha)\left(\left(1+\frac{E_{sp}}{T}\right)\exp\left(-\frac{E_{sp}}{T}\right)-\left(1+\frac{E_{sh}}{T}\right)\exp\left(-\frac{E_{sh}}{T}\right)\right)\right).\end{aligned} \tag{6.6}$$

This can be simplified down to

$$\begin{aligned}\sigma_{\text{th}} = \frac{e}{h}\Bigg(&\alpha\left(-\frac{\mu[c]}{T\left(1+\exp\left(-\mu[c]/T\right)\right)}+\ln\left(1+\exp\left(\frac{\mu[c]}{T}\right)\right)\right)\\&-\alpha\left(\frac{\mu[-c]}{T\left(1+\exp\left(-\mu[-c]/T\right)\right)}+\ln\left(1+\exp\left(\frac{\mu[-c]}{T}\right)\right)\right)\Bigg)\\&+\frac{qe}{h}\left((1-\alpha)\left(\left(1+\frac{E_{sp}}{T}\right)\exp\left(-\frac{E_{sp}}{T}\right)-\left(1+\frac{E_{sh}}{T}\right)\exp\left(-\frac{E_{sh}}{T}\right)\right)\right).\end{aligned} \tag{6.7}$$

It will be this equation that will be used in the later section where the thermopower will be derived from the conductances.

6.2.2 Electrical Conductance

As with the thermal conductance, the electrical conductance is given by the same equation given in chapter 5. This equation is

$$\sigma_{\text{el}} = \frac{\partial I}{\partial \Delta V}. \tag{6.8}$$

but that is where the similarity ends. Because while the temperature at each point across the cross-section of the bar was assumed to be the same in the previous section, the same assumption can not be taken as a given for the voltage drop. This is due to the relationship between the chemical potential, μ and the potential difference across the material. How it changes dependant upon whether the current is travelling through the bulk or the edge states. Therefore how the current is differentiated with respect to the voltage will also have this dependence. This is shown in fig. 6.3.

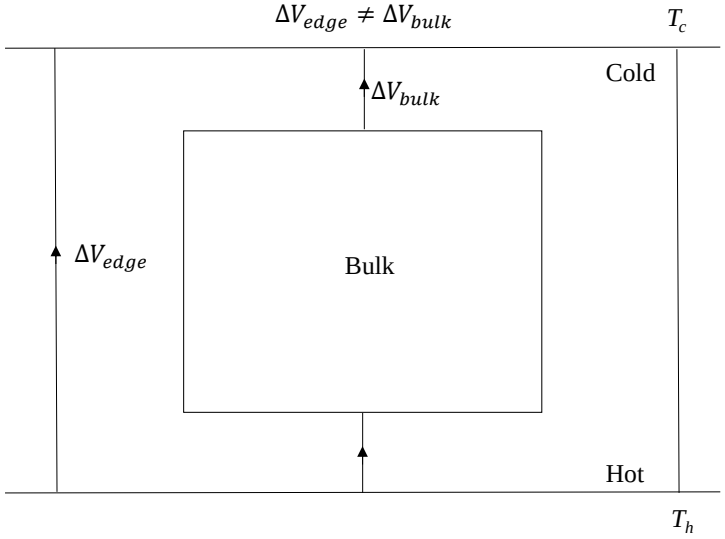

Figure 6.3: A sketch of the system showing how the voltage drop will be different on the edges to the bulk of the material. In this sketch $\Delta V_{\text{edge}} \neq \Delta V_{\text{bulk}}$ due to the variances in the chemical potential.

The voltage drop, ΔV across the system, will be linearly proportional to the current due to Ohms law. From this is it possible to build an equation to define the total ΔV in terms of that across the edges and the bulk, using the current splitting

variable α once more. Therefore this gives

$$\Delta V = \alpha \Delta V_{\text{edge}} + (1-\alpha)\Delta V_{\text{bulk}} \tag{6.9}$$

which in relation to the conductance will transfer to

$$\sigma_{\text{el}} = \frac{\partial I}{\partial(\alpha V_{\text{edge}} + (1-\alpha)V_{\text{bulk}})}, \tag{6.10}$$

when $\Delta V_{edge} \to V_{edge}$ and $\Delta V_{bulk} \to V_{bulk}$ algebraic substitutions are used. This can be simplified as long as the equation is homogeneous, and that the model remains simple in concept. For example, the idea that neither the edge nor the bulk currents contain any inaction term between them is vital. Meaning they only have a dependence upon the voltage drop across there own part of the material. As long as this holds then it is possible to write (6.10) as

$$\sigma_{\text{el}} = \frac{\alpha \partial I_{\text{edge}}}{\alpha \partial V_{\text{edge}}} + \frac{(1-\alpha)\partial I_{\text{bulk}}}{(1-\alpha)\partial V_{\text{bulk}}}, \tag{6.11}$$

which becomes

$$\sigma_{\text{el}} = \frac{\partial I_{\text{edge}}}{\partial V_{\text{edge}}} + \frac{\partial I_{\text{bulk}}}{\partial V_{\text{bulk}}}. \tag{6.12}$$

From this deviation it can be seen that the electrical conductance does not have a dependence on how the current splits. This proves the assumption that was stated at the beginning of this chapter when α was first introduced. The electrical conductance is independent of how the current travels through the system.

To find the electrical conductance of the model being created here, it is first advisable to consider the bulk differentiation. This is due to the simplicity of applying the bulk part of (6.12) to I_{bulk}. This gives

$$\begin{aligned}\frac{\partial I_{\text{bulk}}}{\partial V_{\text{bulk}}} &= \frac{qe}{h}\left(-(qe)\exp\left(-\frac{E_{sp}}{T}\right) - (qe)\exp\left(-\frac{E_{sh}}{T}\right)\right) \\ &= -\frac{qe^2}{h}\left(\exp\left(-\frac{E_{sp}}{T}\right) + \exp\left(-\frac{E_{sh}}{T}\right)\right).\end{aligned} \tag{6.13}$$

Now to look at the edge part of (6.12), the voltage differential once more needs to be converted into the differentiation with respect to μ. So using the same equation given in chapter 5, section 5.3, it can be taken that

$$\frac{\partial}{\partial V_{\text{edge}}} = -\frac{e}{2}\frac{\partial}{\partial \mu}. \tag{6.14}$$

This will give the differential of the edge current to be

$$\begin{aligned}\frac{\partial I_{\text{edge}}}{\partial V_{\text{edge}}} &= -\frac{e^2 \exp\left(\frac{\mu[c]}{T}\right)}{2h\left(1+\exp\left(\frac{\mu[c]}{T}\right)\right)} - \frac{e^2 \exp\left(\frac{\mu[-c]}{T}\right)}{2h\left(1+\exp\left(\frac{\mu[-c]}{T}\right)\right)} \\ &= -\frac{e^2}{2h}\left(\frac{1}{1+\exp\left(\frac{-\mu[c]}{T}\right)} + \frac{1}{1+\exp\left(\frac{-\mu[-c]}{T}\right)}\right). \end{aligned} \tag{6.15}$$

Therefore the electrical conductance is given by

$$\begin{aligned}\sigma_{\text{el}} =& -\frac{qe^2}{h}\left(\exp\left(-\frac{E_{sp}}{T}\right) + \exp\left(-\frac{E_{sh}}{T}\right)\right) \\ & -\frac{e^2}{2h}\left(\frac{1}{1+\exp\left(\frac{-\mu[c]}{T}\right)} + \frac{1}{1+\exp\left(\frac{-\mu[-c]}{T}\right)}\right)\end{aligned} \tag{6.16}$$

6.2.3 Thermopower Equation

Now using the two conductances found in the previous sections, it is possible to construct an equation for the thermopower, using the relationship that

$$S_{xx} = -\frac{\sigma_{\text{th}}}{\sigma\text{el}}. \tag{6.17}$$

Therefore S_{xx} becomes

$$\begin{aligned}S_{xx} =& \frac{e\alpha\left(-\frac{\mu[c]}{T\left(1+e^{-\frac{\mu[c]}{T}}\right)} + \ln\left(1+e^{\frac{\mu[c]}{T}}\right) - \frac{\mu[-c]}{T\left(1+e^{-\frac{\mu[-c]}{T}}\right)} + \ln\left(1+e^{\frac{\mu[-c]}{T}}\right)\right)}{qe^2\left(e^{-\frac{E_{sp}}{T}} + e^{-\frac{E_{sh}}{T}}\right) + \frac{e^2}{2}\left(\frac{1}{1+e^{\frac{-\mu[c]}{T}}} + \frac{1}{1+e^{\frac{-\mu[-c]}{T}}}\right)} \\ &+ \frac{qe\,(1-\alpha)\left(\left(1+\frac{E_{sp}}{T}\right)e^{-\frac{E_{sp}}{T}} - \left(1+\frac{E_{sh}}{T}\right)e^{-\frac{E_{sh}}{T}}\right)}{qe^2\left(e^{-\frac{E_{sp}}{T}} + e^{-\frac{E_{sh}}{T}}\right) + \frac{e^2}{2}\left(\frac{1}{1+e^{\frac{-\mu[c]}{T}}} + \frac{1}{1+e^{\frac{-\mu[-c]}{T}}}\right)}.\end{aligned} \tag{6.18}$$

This equation can be simplified using a few different methods. The first is to insert the fact that $qe = e/4$, and cancel out the terms which can be removed. The second thing that can be done is to replace the $1/(1+\exp(-x))$ with

$$\left(1+\exp\left(-\frac{\mu}{T}\right)\right)^{-1} \approx 1 - \exp\left(-\frac{\mu}{T}\right) \tag{6.19}$$

which is the expansion to the first order. The next simplification that can be made is to rewrite the $\ln(x)$ term using logarithm rules, such that it becomes

$$\ln\left(1+\exp\left(\frac{\mu}{T}\right)\right) = \frac{\mu}{T} + \ln\left(1+\exp\left(-\frac{\mu}{T}\right)\right). \tag{6.20}$$

This can be simplified even more by using the series expansion on the natural logarithm because $\exp(-x) < 1$. The series expansion of the natural logarithm in this situation is $\ln(1+x) = x + \mathcal{O}(1)...$ when $|x| < 1$. Therefore (6.20) can be written as

$$\ln\left(1+\exp\left(\frac{\mu}{T}\right)\right) = \left(\frac{\mu}{T} + \exp\left(-\frac{\mu}{T}\right)\right). \tag{6.21}$$

Using these simplifications it is possible to rewrite the components in the denominator of (6.18) that come from the edge current, as

$$\begin{aligned} -\frac{\mu}{T\left(1+e^{-\frac{\mu}{T}}\right)} + \ln\left(1+e^{\frac{\mu}{T}}\right) &= -\frac{\mu}{T}\left(1-\exp\left(-\frac{\mu}{T}\right)\right) + \frac{\mu}{T} + \exp\left(-\frac{\mu}{T}\right) \\ &= \left(1+\frac{\mu}{T}\right)\exp\left(-\frac{\mu}{T}\right). \end{aligned} \tag{6.22}$$

This holds for both $\mu[c]$ and $\mu[-c]$. Therefore (6.18) now becomes

$$\begin{aligned} S_{xx} =& \frac{4\alpha\left(\left(1+\frac{\mu[c]}{T}\right)e^{-\frac{\mu[c]}{T}} + \left(1+\frac{\mu[-c]}{T}\right)e^{-\frac{\mu[-c]}{T}}\right)}{qe\left(e^{-\frac{E_{sp}}{T}} + e^{-\frac{E_{sh}}{T}}\right) + \frac{8qe}{1+e^{\frac{-\mu[c]}{T}}} + \frac{8qe}{1+e^{\frac{-\mu[-c]}{T}}}} \\ &+ \frac{(1-\alpha)\left(\left(1+\frac{E_{sp}}{T}\right)e^{-\frac{E_{sp}}{T}} - \left(1+\frac{E_{sh}}{T}\right)e^{-\frac{E_{sh}}{T}}\right)}{qe\left(e^{-\frac{E_{sp}}{T}} + e^{-\frac{E_{sh}}{T}}\right) + \frac{8qe}{1+e^{\frac{-\mu[c]}{T}}} + \frac{8qe}{1+e^{\frac{-\mu[-c]}{T}}}}. \end{aligned} \tag{6.23}$$

The only thing to do now, is to change the units such that the temperature is no longer in energy units. To do this (6.23) needs to be multiplied by k_B. This means the final equation for the thermopower is

$$\begin{aligned} S_{xx} =& \frac{k_B}{qe}\frac{4\alpha\left(\left(1+\frac{\mu[c]}{T}\right)e^{-\frac{\mu[c]}{T}} + \left(1+\frac{\mu[-c]}{T}\right)e^{-\frac{\mu[-c]}{T}}\right)}{e^{-\frac{E_{sp}}{T}} + e^{-\frac{E_{sh}}{T}} + \frac{8}{1+e^{\frac{-\mu[c]}{T}}} + \frac{8}{1+e^{\frac{-\mu[-c]}{T}}}} \\ &+ \frac{k_B}{qe}\frac{(1-\alpha)\left(\left(1+\frac{E_{sp}}{T}\right)e^{-\frac{E_{sp}}{T}} - \left(1+\frac{E_{sh}}{T}\right)e^{-\frac{E_{sh}}{T}}\right)}{e^{-\frac{E_{sp}}{T}} + e^{-\frac{E_{sh}}{T}} + \frac{8}{1+e^{\frac{-\mu[c]}{T}}} + \frac{8}{1+e^{\frac{-\mu[-c]}{T}}}}. \end{aligned} \tag{6.24}$$

6.3 Thermopower

The thermopower equation found in the previous section is one that describes the simple model of the system being looked at. This means that it does not involve tunnelling. Which in turn leads to the fact that the equation given in chapter 5, for the transition value, can not be used. This is because without tunnelling the variation in the conductance is not noticeable along the plateau. But the transition value is still an important variable in the equation which defines the chemical potential. Therefore the transition value, c, will be treated as a free parameter in this section as the results from the simple model are investigated, and compared to those experimentally found in [3]. This idea will be looked at in great depth in the next section.

The equations that will be used within the themopower to express the chemical potential, μ, the particle energy, E_{sp}, and the hole energy, E_{sh} are

$$E_{sp} = (1-g)\frac{\Delta}{2}, \qquad E_{sh} = (1+g)\frac{\Delta}{2}, \qquad \mu = (1-cg)\,\frac{\Delta}{2}, \tag{6.25}$$

where

$$g = \frac{\delta\nu}{\delta\nu_m}. \tag{6.26}$$

$\delta\nu_m$ is the maximum value of the filling factor along the plateau, and $\delta\nu$ is how it varies as the particle move across it this is shown in fig.6.4. It is g that the themopower will be plotted against, as the model being developed only holds across the plateau. Therefore how this variable relates to the magnetic field values needs to be determined so that the result can be compared to those found through experiments.

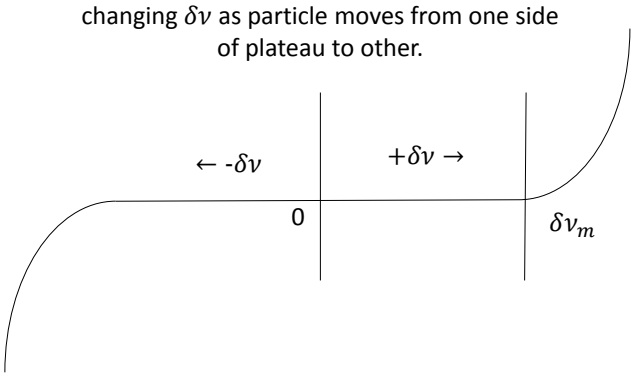

Figure 6.4: A sketch of a plateau showing $\delta\nu_m$ and how the $\delta\nu$ will change as it moves across it.

From [6] it is known that as $\delta\nu$ increases from the centre of the plateau, when $g = 0$, then the transport will be dominated by electrons. This shows that the saddle point heights the particles need to cross, E_{sp}, will become lower the further along the plateau it travels. So this agrees with (6.25) as obviously E_{sp} will vanish when $\nu \to \nu = \nu_m + \delta\nu_m$. The reverse is also true in the fact that the holes behave in the opposite way. As $\delta\nu$ decreases from the centre of the plateau E_{sh} decreases and therefore holes become the dominate from of transport. As such E_{sh} vanishes as $\nu \to \nu = \nu_m - \delta\nu_m$ which is therefore when g is negative.

It has been stated previously that [4]

$$\nu = \frac{nh}{eB}. \tag{6.27}$$

Therefore to see how g_ν relates to the magnetic field, this relation can be used. So take

$$g_\nu = \frac{\delta\nu}{\delta\nu_m} \qquad \text{and} \qquad g_B = \frac{\delta B}{\delta B_m} \tag{6.28}$$

(6.27) can be used to turn $\delta\nu \to \delta B$ and $\delta\nu_m \to \delta B_m$. This is done by considering

$$\delta\nu_m = \nu_m - \nu_{min} \tag{6.29}$$

$$\delta B_m = B_m - B_{min}. \tag{6.30}$$

Using (6.27) then it is possible to rewrite (6.29) to be

$$\begin{aligned}
\delta\nu_m &= \frac{nh}{eB_m} - \frac{nh}{eB_{min}} \\
&= \frac{nh}{e}\left(\frac{1}{B_m} - \frac{1}{B_{min}}\right) \\
&= \frac{nh}{e}\frac{B_{min} - B_m}{B_m B_{min}} \\
&= -\frac{nh}{e}\frac{\delta B_m}{B_m B_{min}}.
\end{aligned} \tag{6.31}$$

Putting this into (6.28) for g_ν gives

$$g_\nu = -\frac{e}{nh}\frac{\delta\nu}{\delta B_m} B_m B_{min}. \tag{6.32}$$

This same process can be applied to the change $\delta\nu \to \delta B$. Therefore this becomes

$$\begin{aligned}\delta\nu &= \nu_m - \nu' \\ &= \frac{nh}{eB_m} - \frac{nh}{eB'} \\ &= -\frac{nh}{e}\frac{\delta B}{B_m B'}.\end{aligned} \tag{6.33}$$

So putting this in (6.32) gives

$$\begin{aligned}g_\nu &= \frac{\delta B}{\delta B_m}\frac{B_{min}}{B'} \\ &= g_B\frac{B_{min}}{B'}.\end{aligned} \tag{6.34}$$

Now because the width of the plateau, the distance between B_{min} and B_{max}, is small then it is possible to approximate $\frac{B_{min}}{B'} \approx 1$. So therefore the relationship between the g's is $g_\nu = g_B$. So when looking at the graphs this model will produce, then $\frac{\delta\nu}{\delta\nu_m}$ can be interchanged with $\frac{\delta B}{\delta B_m}$. As such the direction of g along the x-axis, follows the direction of B. The model will also produce the graphs so that they follow the experimental convention of having $-S_{xx}$ on the top of the y-axis. This is shown in fig.6.5.

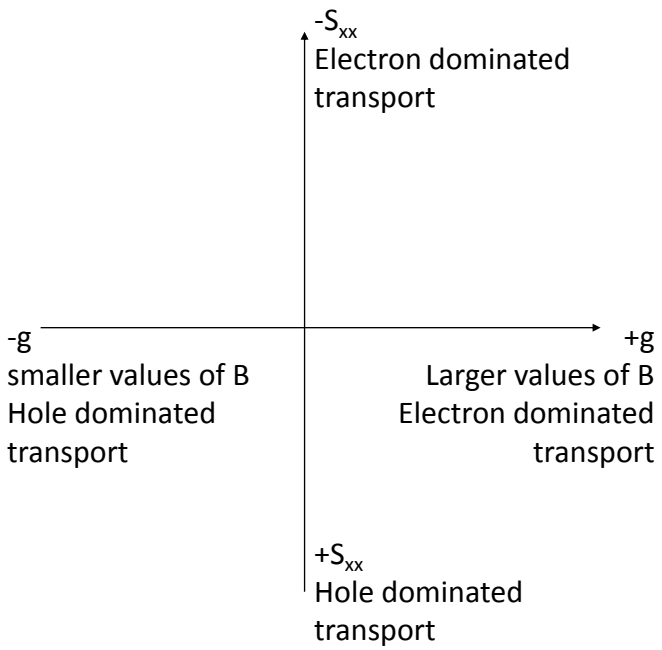

Figure 6.5: How g relates to the magnetic field, B, and how this relates to electron or hole domination in the transport through the material. It also includes the general conventions for the expression of the thermopower, S_{xx}.

6.3.1 Changing The Transition Value

As stated previously the transition value c cannot be calculated using the equation derived in chapter 5 in this simple model. Instead it is a free parameter. This means that its value will need to be determined by running the model for a set temperature and energy gap, and the range of current splitting, α, values. This is done in fig.6.6, where the different graphs are shown for values of $c = [0, 1]$ in increments of 0.1. The different coloured trajectories show how the thermpower changes with α for each value of c. The value of α that corresponds to each coloured line is given in table 6.1.

α	Colour	α	Colour	α	Colour	α	Colour
0.0	Red	0.1	Blue	0.2	Green	0.3	Black
0.4	Gray	0.5	Cyan	0.6	Magenta	0.7	Orange
0.8	Brown	0.9	Purple	1.0	Pink		

Table 6.1: The table showing how the different α values correspond to the different coloured lines in fig.6.6.

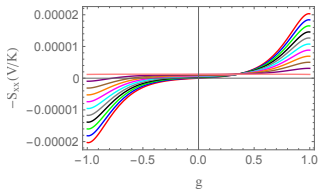

(a) Thermopower S_{xx}, with $c = 0$, $\Delta/T = 14$.

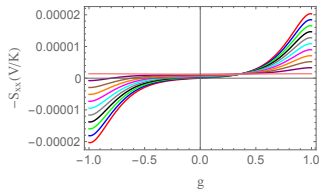

(b) Thermopower S_{xx}, with $c = 0.1$, $\Delta/T = 14$.

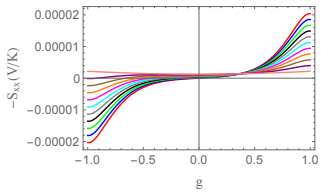

(c) Thermopower S_{xx}, with $c = 0.2$, $\Delta/T = 14$.

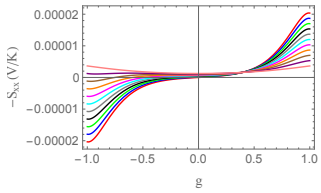

(d) Thermopower S_{xx}, with $c = 0.3$, $\Delta/T = 14$.

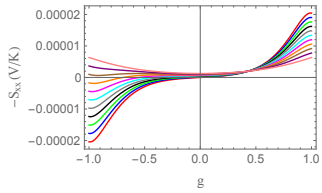

(e) Thermopower S_{xx}, with $c = 0.4$, $\Delta/T = 14$.

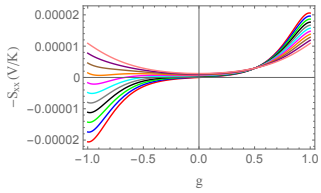

(f) Thermopower S_{xx}, with $c = 0.5$, $\Delta/T = 14$.

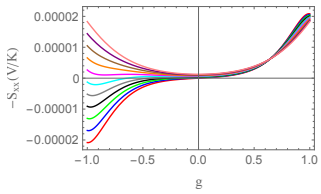

(g) Thermopower S_{xx}, with $c = 0.6$, $\Delta/T = 14$.

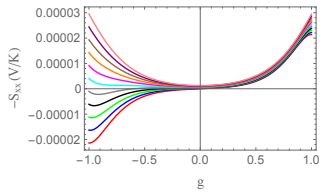

(h) Thermopower S_{xx}, with $c = 0.7$, $\Delta/T = 14$.

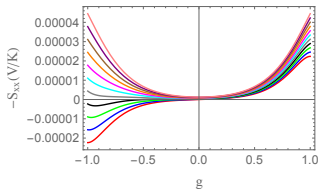

(i) Thermopower S_{xx}, with $c = 0.8$, $\Delta/T = 14$.

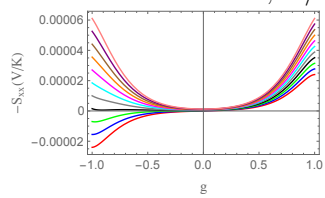

(j) Thermopower, S_{xx} with $c = 0.9$, $\Delta/T = 14$.

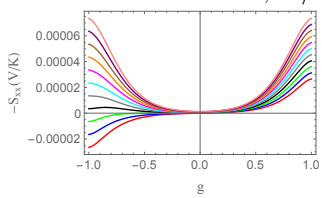

(k) Thermopower S_{xx}, with $c = 1$, $\Delta/T = 14$.

Figure 6.6: Plots showing how the thermopower changes with the different values of the transition value c, for $\Delta/T = 14$, and the current splitting parameter α. Which lies in the range of $\alpha = [0, 1]$ in 0.1 increments.

It can be seen from fig.6.6 that for smaller values of the transition value c, the results given by the model do not tally with those gained in experimentation. Therefore from this is it possible to deduce, for this simple model, that the value of c that needs to be taken is of a larger value than 0.5. As such for the rest of this chapter, the value of c that will be used is $c- = 0.8$ due to the fact that this is the graph that resembles the experimental results given in chapter 2 the closest for the $\Delta/T = 14$ value.

6.3.2 Changing The Temperature

The previous section suggested an approximate value for the transition value c, which means the model can now be tested against the changing value of the temperature. It is known how the model should behave, the higher the temperature the less pronounced the plateau, and as such the less the dip in the thermopower will be. Therefore the model shall be run over a range of temperatures, which will be represented by the changing value of Δ/T. This is due to the fact that the energy gap Δ will not change as the temperature does. These results are given in fig.6.7 and fig.6.8. The different colours in the graphs represent the different values of current splitting parameter α and correspond to the those given in table 7.1.

α	Colour	α	Colour	α	Colour	α	Colour
0.0	Red	0.1	Blue	0.2	Green	0.3	Black
0.4	Gray	0.5	Cyan	0.6	Magenta	0.7	Orange
0.8	Brown	0.9	Purple	1.0	Pink		

Table 6.2: The table showing how the different α values correspond to the different coloured lines in fig.6.7 and fig.6.8.

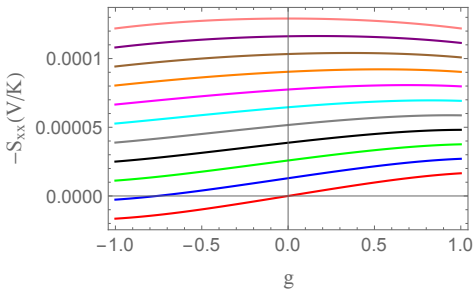

(a) Thermopower S_{xx}, with $c = 0.8$, $\Delta/T = 2$.

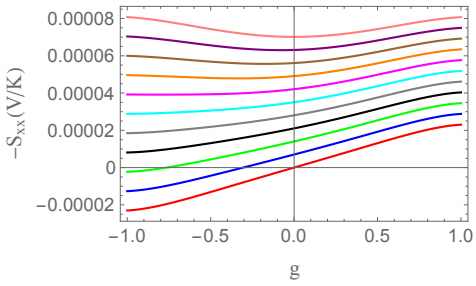

(b) Thermopower S_{xx}, with $c = 0.8$, $\Delta/T = 4$.

Figure 6.7: Plots showing how the thermopower changes with the different values of the temperature T, for $c = 0.8$, and the current splitting parameter α. Which lies in the range of $\alpha = [0, 1]$ in 0.1 increments.

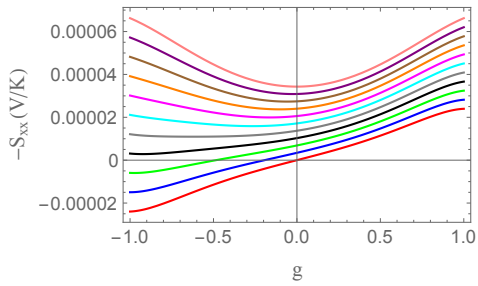

(a) Thermopower S_{xx}, with $c = 0.8$, $\Delta/T = 6$.

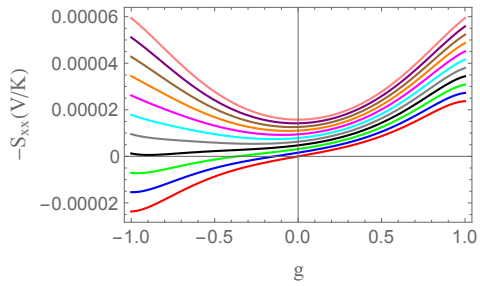

(b) Thermopower S_{xx}, with $c = 0.8$, $\Delta/T = 8$.

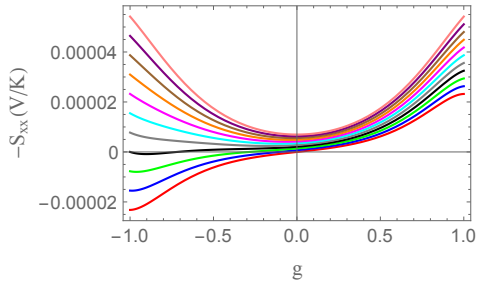

(c) Thermopower S_{xx}, with $c = 0.8$, $\Delta/T = 10$.

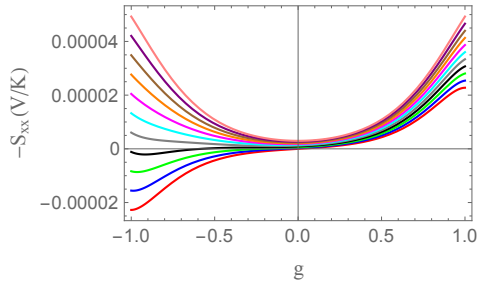

(d) Thermopower S_{xx}, with $c = 0.8$, $\Delta/T = 12$.

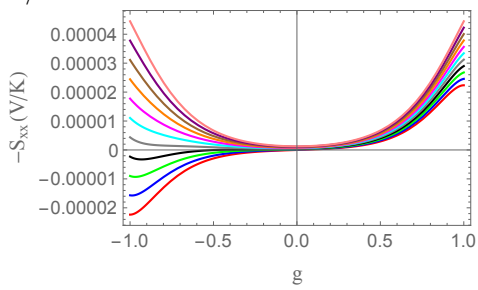

(e) Thermopower S_{xx}, with $c = 0.8$, $\Delta/T = 14$.

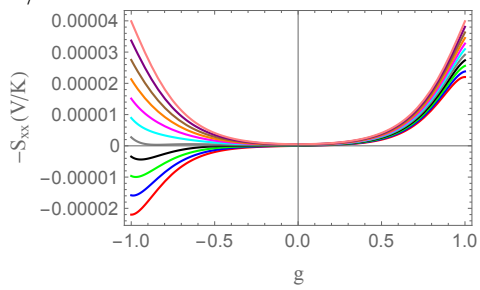

(f) Thermopower S_{xx}, with $c = 0.8$, $\Delta/T = 16$.

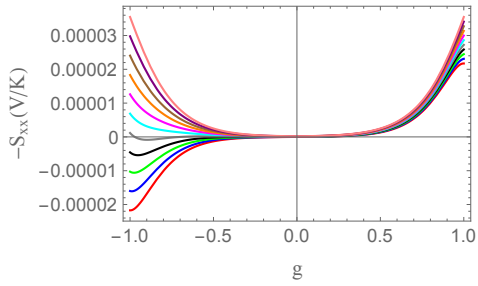

(g) Thermopower S_{xx}, with $c = 0.8$, $\Delta/T = 18$.

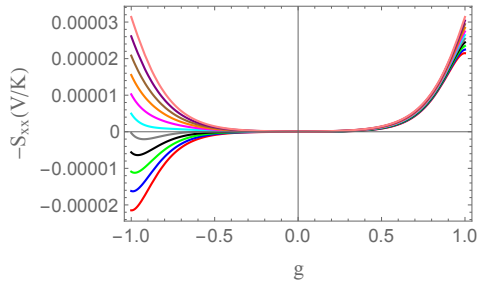

(h) Thermopower, S_{xx} with $c = 0.8$, $\Delta/T = 20$.

Figure 6.8: Plots showing how the thermopower changes with the different values of temperature with the transition value $c = 0.8$, and the current splitting parameter α. Which lies in the range of $\alpha = [0, 1]$ in 0.1 increments.

It can be seen from fig.6.8g and fig.6.8h that as the value of Δ/T increases the model will return the same values for the thermopower. This is because these values are representative of extremely low temperatures, and in the real system, the thermoelectric transport will be dominated by tunnelling. And as this simple model does not include this phenomenon then it stagnates at the point where tunnelling will take over from the more classical forms of transport. But despite this upper threshold, the graphs for the lower values of Δ/T, and thus higher temperatures, for example fig.6.7a and fig.6.7b show that at these points the plateau which causes the thermopower to drop off, has not yet formed. As the temperature lowers through figs.6.8a, 6.8b and 6.8c that drop off, and therefore the plateau formation, can be seen. This shows that the model does work, within the limit that it was created to preform at, and as such it can be used as a tentative example to check against the experimental data found in [3].

6.4 Comparison With Experimental Data

To compare the result from the model with those found experimentally by Chickering et al.[3] a particular filling factor needs to be chosen. One which has plenty of experimental data to give a robust comparison for the simplified model. The one that is most investigated in [3] is the 5/2 state as this is the one which has no confirmed theory to describe the behaviour of the particles. As such the 5/2 is the one that will be used to compare the results from the model developed, to make sure that it is within an acceptable tolerance for the parameters being investigated. Especially as this state is the one that the model hopes to explain the behaviour of in greater detail.

To do this comparison then the value of α for the system needs to be chosen, as this is the only true free parameter. Therefore firstly the value of Δ/T for the simplified model, which corresponds to the different temperatures measured experimentally, has to be found. This is done by using the measured value of Δ from [3], which is given to be $\Delta \approx 430$mK. This gives the values for Δ/T to be $\Delta/T \approx 10.5$, 15, 21.5 for the temperatures $T = 41$mK, 28mK, 20mK respectively.

The experimental data and the theoretical model graphs are both shown in fig.8.2. It can be seen from this graphic that while the model gives the correct shape for the different temperatures, the value of the thermopower $-S_{xx}$ is out by a factor of 10. This noticeable difference between fig.8.3a and fig.8.2b is due to the fact that the theoretical model is a simplified one. It therefore does not include tunnelling which, at the low temperatures being looked at, is the dominate form of transport

within the material. As such while it can not be said with complete certainty that this model will give an appropriate theoretical deviation of the thermopower at low temperatures, it does show that it gives the correct behaviour, even if the range is off by a factor of 10 due to the lack of tunnelling.

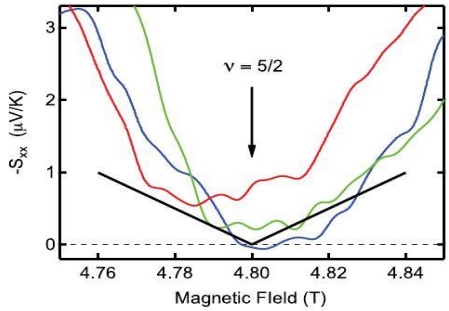

(a) Thermopower data for the 5/2 state from [3]. The black line shows a different gtheoretical prediction by Yang and Halperin [40].

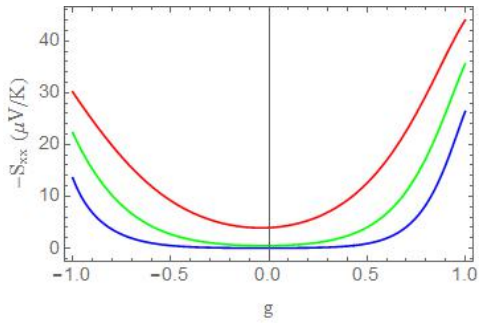

(b) Thermopower from the simplified model with $c = 0.8$ and $\alpha = 0.7$.

Figure 6.9: Plots showing how the thermopower changes with the different values of temperature for both the experimental data and the simplified model. The different coloured lines are for the different temperatures, blue=20mK, green=28mK, and red=41mK.

In the next chapter, this simplified model will be developed to include tunnelling.

Chapter 7

Inclusion of Tunnelling

The tunnelling effects the derived conductances depending on the ratio Δ/T. In the very low temperatures of the quantum Hall regime, Δ/T is high and as such tunnelling will play a large part in the derivation of the thermopower. This is because at these low temperatures the particles and holes do not have the energy required to move over the barriers the saddle points represent, Thus majority of the particle and hole movement is via tunnelling. This will make the effective average value of the saddle point height be lower than it is when dealt with classically, as in the classical regime the particles can either go over the saddle point or they get scattered back. But in the regime we are looking at, they can also tunnel through, effectively cutting off the top of the saddle point and making its value lower. This is shown in fig.7.1.

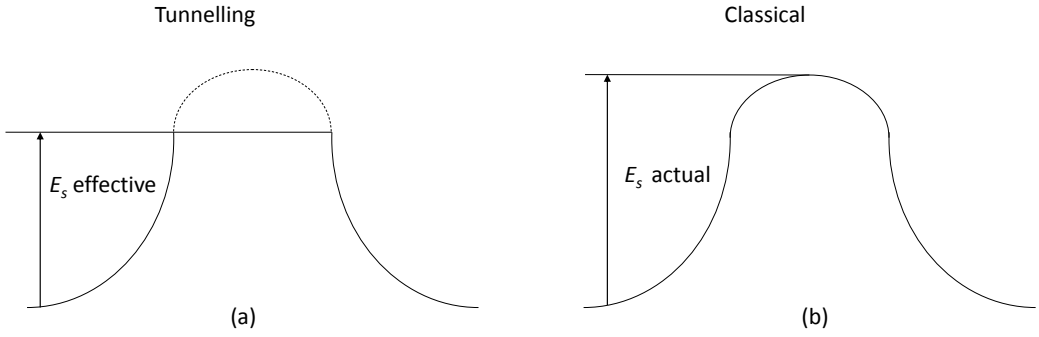

Figure 7.1: A sketch showing how the tunnelling reduces the actual energy gap value E_s, shown in (b), to an effective one, shown in (a).

To include tunnelling, and thus this effective value for the energy gap into the equation for the thermopower model found in chapter 6, so that the behaviour of the particle and holes at low temperatures is taken into account. It has been

found previously in [41] and [6] that the equation for the transmission probability through the bulk, $\mathcal{T}(E-E_s)$, with respect to tunnelling for the specific saddle point potential $W(x) = E_s - U_x x^2 + U_y y^2$ is given by

$$\mathcal{T}(E - E_s) = \frac{1}{1 + \exp\left(\frac{-\pi(E-E_s)}{l_q^2\sqrt{U_x U_y}}\right)}. \tag{7.1}$$

This is relevant as this specific potential is the one used when modelling the system as a network of resistors, as is being done here. Now $\sqrt{U_x U_y}$ can be replaced by $\Delta_s/2a^2$, where Δ_s is the energy gap of the saddle point, whereas E_s is the energy connected to the particles transport across the saddle, as explained previously in this thesis. Therefore (7.1) will become

$$\mathcal{T}(E - E_s) = \frac{1}{1 + \exp\left(\frac{-\pi 2a^2(E-E_s)}{l_q^2\Delta_s}\right)}. \tag{7.2}$$

where the variable a^2/l_q^2 is the tunnelling coefficient, and is comprised of a, which is the half the width between the different puddles, and as such is half the width of the saddle point, and l_q is the magnetic length of the quasi-particles or quasi-holes. This is the part which dictates how much tunnelling is happening in the system. For lower values of the tunnelling coefficient, which will be referred to as γ throughout the rest of this thesis, tunnelling becomes the main form of transport across the saddle points, and as such this transmission probability takes control. Whereas for higher values of γ this will approximate to the simplified system already proposed where tunnelling is not taken into account, as such the probability equation will revert back to where $\mathcal{T}$ will equal either 0 or 1, depending on whether the particle has the energy to transverse the gap. This is because the particles will have the energy to cross the saddle in the normal ways, and that will become the most dominate form of transportation. With the new notation given, (7.2) will become

$$\mathcal{T}(E - E_s) = \frac{1}{1 + \exp\left(-2\pi\gamma^2\frac{(E-E_s)}{\Delta}\right)}. \tag{7.3}$$

In the following sections, how this equation changes the conductance will be investigated and a new, more complex model, will be derived to model the thermopower.

7.1 The Behaviour of The Conductance

The equation to find the number current of the system using (7.3) for the transmission probability in (3.1) is given by

$$i_{lr} = \frac{1}{h}\int_0^{\Delta} dE\, \frac{\exp\left(-E/T\right)}{1+\exp(-2\pi\gamma^2\frac{(E-E_s)}{\Delta})}. \tag{7.4}$$

which gives the equation for the conductance σ to be [33]

$$\sigma = \frac{(qe)^2}{hk_BT}\int_0^{\Delta} dE\, \frac{\exp\left(-E/T\right)}{1+\exp\left(-2\pi\gamma^2\frac{(E-E_s)}{\Delta}\right)}. \tag{7.5}$$

To evaluate this, the variable being integrated over needs to change into those of known parameters. As such the change in variable will be

$$E = x\Delta, \tag{7.6}$$

this change makes the exponential in the denominator become

$$\exp(-2\pi\gamma^2\frac{(E-E_s)}{\Delta}) = \exp(-2\pi\gamma^2(x-x_s)), \tag{7.7}$$

and the one in the numerator to transform to

$$\exp\left(\frac{E}{T}\right) = \exp\left(\frac{E}{\Delta}\frac{\Delta}{T}\right) = \exp\left(x\frac{\Delta}{T}\right). \tag{7.8}$$

The final conversation that needs to take place is that of the integral variable and the limits of integration.

$$\frac{dE}{dx} = \Delta \qquad \text{therefore} \qquad dE = \Delta dx, \tag{7.9}$$

and the limits change such that

$$\begin{aligned} 0 &\to \frac{0}{\Delta} \to 0 \\ \Delta &\to \frac{\Delta}{\Delta} \to 1. \end{aligned} \tag{7.10}$$

Putting (7.7), (7.8),(7.9) and (7.10) into (7.5) then the conductance becomes

$$\sigma = \frac{(qe)^2}{hk_B}\frac{\Delta}{T}\int_0^1 dx\, \frac{\exp\left(-x\Delta/T\right)}{1+\exp(-2\pi\gamma^2(x-x_s))} \tag{7.11}$$

which can be evaluated numerically for various different values of γ and Δ/T. The variable x_s is the one which will relate to the variables E_{sp} for particles and E_{sh} for holes. Using (7.6) this relationship can be seen to be $x_s = E_s/\Delta$. This will give the values for $E_{sp} \to x_{sp}$, and $E_{sh} \to x_{sh}$ to be $x_{sp} = (1-g)/2$ and $x_{sh} = (1+g)/2$ respectively. The centre of the plateau will be taken when $x_s = 1/2$. Figure 7.2 shows the numerically evaluated conductance for different values of γ, at the centre of the plateau.

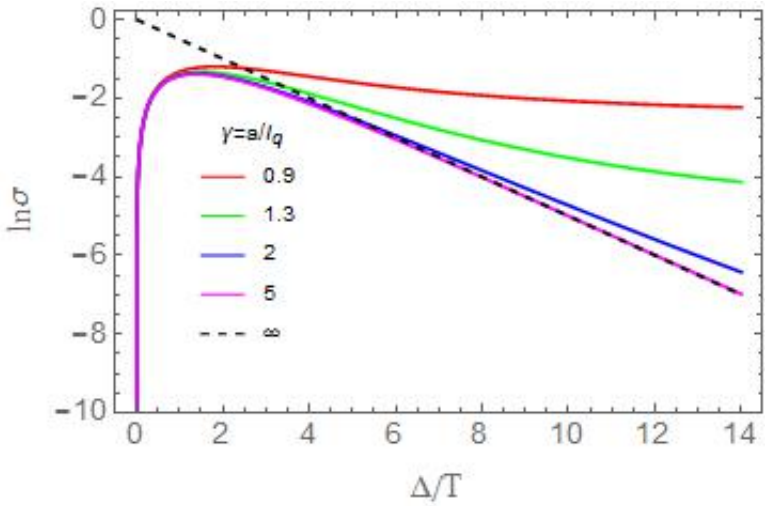

Figure 7.2: a plot of the log of the thermal conductance for changing values of Δ/T. done at different values of γ. the line colours equate to, red: $\gamma = 0.9$, green: $\gamma = 1.3$, blue: $\gamma = 2$ and Magenta: $\gamma = 5$. The Dashed black line is the result given by the equation found in [4] without tunnelling.

From this plot it can be seen that as γ increases in value it approaches the result found previously without tunnelling. Whereas for smaller values of γ and larger values of Δ/T then the result varies greatly from that found using a more classical approach. This shows that this model performs the required transition from the semi-classical, thermal excitation dominated approximation at higher γ values, to one which is dominated by tunnelling in the lower end of the regime.

7.2 Deriving The Thermopower

The total current for the system being investigated will change with the inclusion of tunnelling. This change will affect the bulk current as the equation taken from [6] assumed that the transmission probability $\mathcal{T}(E - E_s)$ was either 0 or 1. In this

section that assumption no longer holds. Therefore the bulk current will become

$$I_{\text{bulk}} = \frac{\Delta qe}{h} \int_0^1 dx \, \frac{\exp\left(-x\frac{\Delta}{T}\right)}{1 + \exp(-2\pi\gamma^2(x - x_s))}. \tag{7.12}$$

The edge current will remain the same as that found in chapter 5 due to the fact that the tunnelling mainly happens in the bulk of the material. The easiest way to evaluate (7.12) for inclusion into the thermopower is to first derive the conductances equations before integration. The electrical conductance is the one already looked into previously (7.13) and as is therefore given by

$$\sigma_{\text{el}} = \frac{(qe)^2}{hk_B} \frac{\Delta}{T} \int_0^1 dx \, \frac{\exp\left(-x\Delta/T\right)}{1 + \exp(-2\pi\gamma^2(x - x_s))}. \tag{7.13}$$

The thermal conductance will need to be derived from (7.12). This is relatively easy as the only component in the equation that has any dependence on the temperature is the exponential in the numerator. Therefore the thermal conductance, σ_{th} will be given by

$$\begin{aligned} \sigma_{\text{th}} &= \frac{\partial}{\partial T} \left(\frac{\Delta qe}{h} \int_0^1 dx \, \frac{\exp\left(-x\frac{\Delta}{T}\right)}{1 + \exp(-2\pi\gamma^2(x - x_s))} \right) \\ &= \left(\frac{\Delta}{T}\right)^2 \frac{qe}{h} \int_0^1 dx \, \frac{x \exp\left(-x\frac{\Delta}{T}\right)}{1 + \exp(-2\pi\gamma^2(x - x_s))}. \end{aligned} \tag{7.14}$$

Both these equations when integrated will produce hypergeometric functions ${}_2F_1$, which require numerical evaluation. As such no complete equation for the thermopower can be written down. But it can be expressed as shown in (7.15) where the electrical and thermal conductances for the edge states are those determined. Therefore the thermopower power becomes

$$S_{xx} = -\frac{(1-\alpha)\sigma_{\text{th},sp} - (1-\alpha)\sigma_{\text{th},sh} + \alpha\sigma_{\text{th,edge},+c} + \alpha\sigma_{\text{th,edge},-c}}{\sigma_{\text{el},sp} - \sigma_{\text{el},sh} + \sigma_{\text{el,edge},+c} + \sigma_{\text{el,edge},-c}}. \tag{7.15}$$

To show that this does indeed work, fig. 7.3 shows how the inclusion of tunnelling will change the behaviour of the thermopower through the bulk of the material only. It can be seen that there is a difference in not just the values, but also the behaviour as the particles move across the plateau.

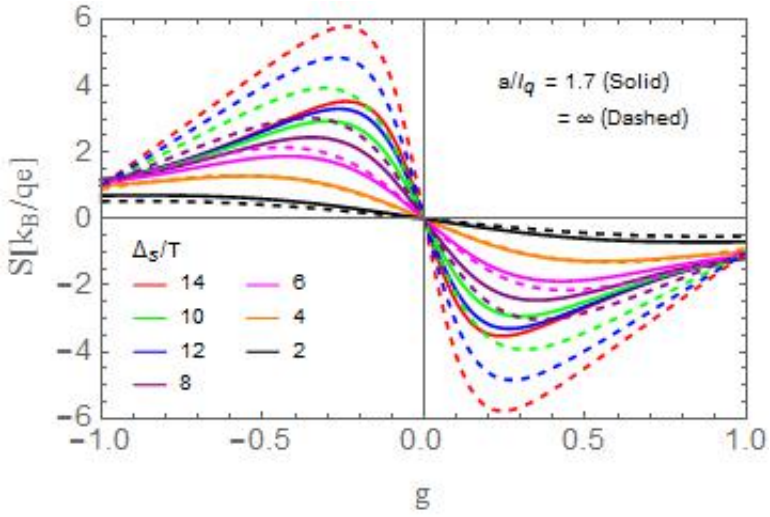

Figure 7.3: The thermopower for the bulk of the system where the dashed lines are those given from the simplified model discussed in chapter 6, whereas the solid lines are including tunnelling. this is modelled in the corbino geometry and developed in [6].

The γ value used here is one that is in the middle of the possible values. It is not an extreme amount of tunnelling, but there is enough to show the different behaviour of the particles in such a regime.

7.3 Thermopower

In the following sections the model for the thermopower will be run for different values of temperature, given by varying the value of Δ/T. The smaller the value of Δ/T then the higher the temperature. Those will be the systems that have less tunnelling and as such behave in the way shown in the simplified model in chapter 6. The difference will be that this time the transition parameter c will be calculated using the equation derived in chapter 5. α is still a free parameter that needs to be determined by comparing the results given by the model with those found experimentally. Thus all the plots in the sections to follow will include the different possible values of α. The γ values that will be used to investigate the behaviour of this system, and to confirm the robustness of the model, will range between $\gamma = [1, 2]$. These are the values that will show the effect of tunnelling well, and will also be able to be compared the results with experimental data. In all the graphs shown below the colours of the different lines correspond to the values of α as given in 7.1.

α	Colour	α	Colour	α	Colour
0.1	Blue	0.2	Green	0.3	Black
0.4	Gray	0.5	Cyan	0.6	Magenta
0.7	Orange	0.8	Brown	0.9	Purple

Table 7.1: The table showing how the different α values correspond to the different coloured lines in the following sections.

7.3.1 $\Delta/T = 10$

The first value is $\Delta/T = 10$, and corresponds to approximately 40mK. At this temperature it is expected that tunnelling will be present, but it may not be the dominate form of transport. This is shown in fig.7.4 as it can be seen that while the fractional quantum Hall states are appearing, the unusual phenomena of the thermopower changing sign does not appear.

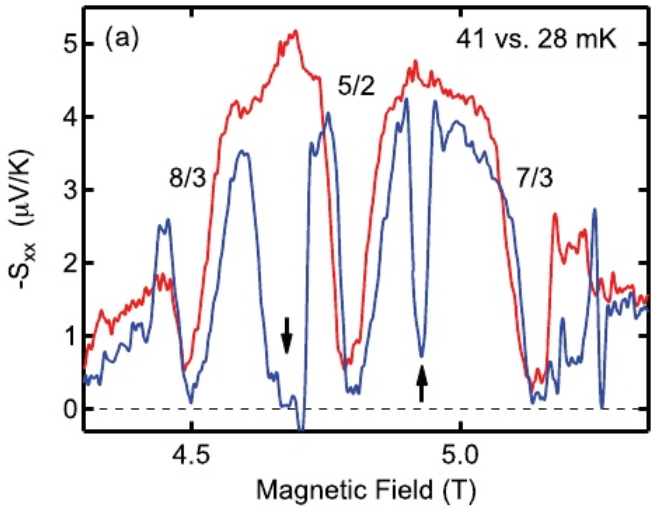

Figure 7.4: The data published in [3] showing the difference in behaviour of the thermopower at both 41mK (the red line), and 28mK (the blue line).

The model developed in this thesis, should be able to predict this behaviour within reasonable accuracy, depending upon the free parameters α and γ. The range of $\alpha = [0.1, 0.9]$ will be run for each value of γ and the different γ's are $\gamma = 1.1$, 1.3, 1.5, 1.7, 1.9. The value for the transition value, c, will also change for each different γ value, as it is dependant upon the conductance. Each of these values are declared under each graph in fig.7.5.

(a) $\gamma = 1.1$ and $c = 0.69$.

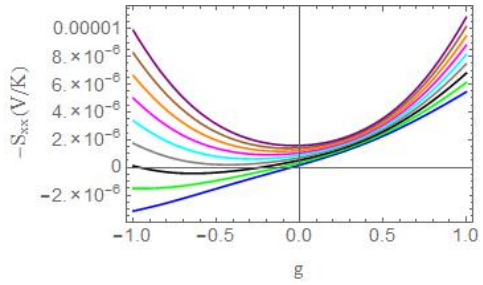

(b) $\gamma = 1.3$ and $c = 0.60$.

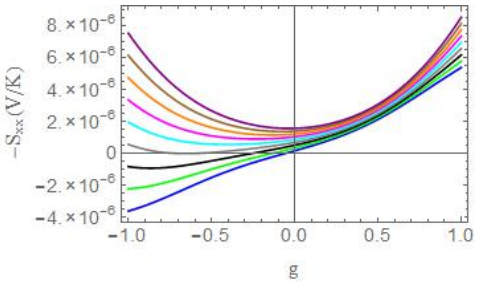

(c) $\gamma = 1.5$ and $c = 0.53$.

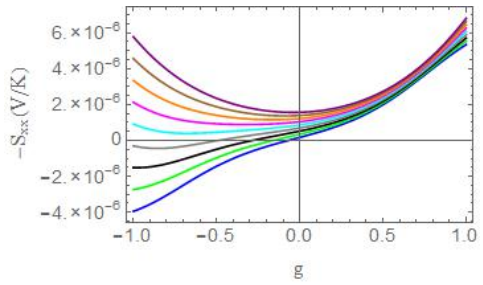

(d) $\gamma = 1.7$ and $c = 0.46$.

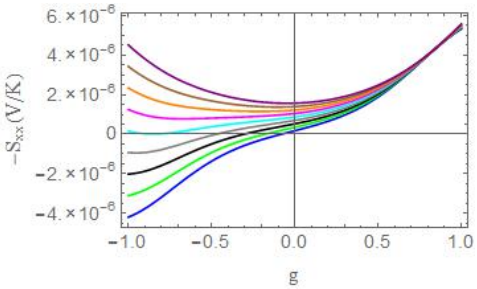

(e) $\gamma = 1.9$ and $c = 0.40$.

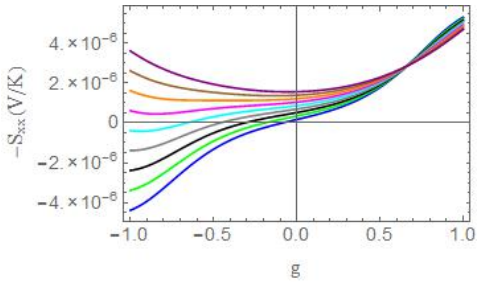

Figure 7.5: The results from the model for different γ values, where $\Delta/T = 10$.

Fig.7.5 shows that the higher the γ value the lower the value for the transition value c, as well as the model giving a flat behaviour across the plateau. Whereas for the lower values, a definite curve can be seen. This is due to the model showing how the dip in the thermopower at the filling factor increases as the tunnelling does. The difference in behaviour from a bulk dominated to edge dominated thermopower is also observed, with the blue line showing how the bulk domination is the reason for the thermopowers sign change. Meaning that for $-g$, the bulk behaviour is dominated by the hole transport. Whereas the purple shows that the edge dominated regime remains completely positive, and thus is dictated by particles.

7.3.2 $\Delta/T = 15$

The value of $\Delta/T = 15$ corresponds to a temperature of approximately 30mK. This is a temperature at which tunnelling is involved in the transport of the particle throughout the system, and as such should have a γ value that is within this activated range. Once again the α values will be varying across the range of $\alpha = [0.1, 0.9]$ and the γ values the model will be run for are $\gamma = 1.1, 1.3, 1.5, 1.7, 1.9$. The transition value will be the one that corresponds to these different γ's. The results from the model are shown in fig.7.6.

(a) $\gamma = 1.1$ and $c = 0.77$.

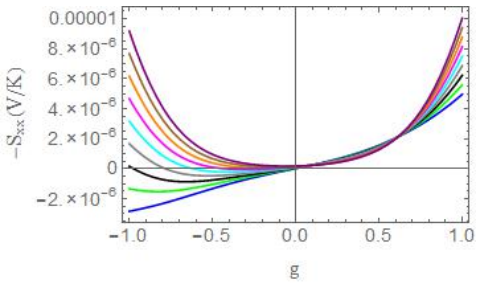

(b) $\gamma = 1.3$ and $c = 0.70$.

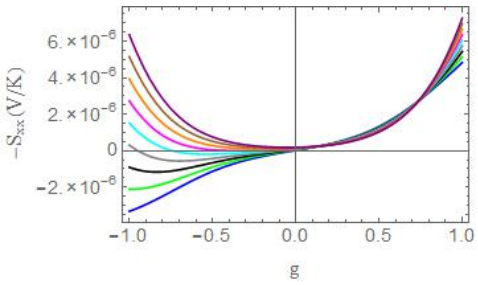

(c) $\gamma = 1.5$ and $c = 0.63$.

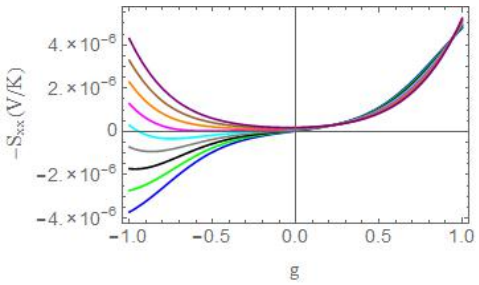

(d) $\gamma = 1.7$ and $c = 0.57$.

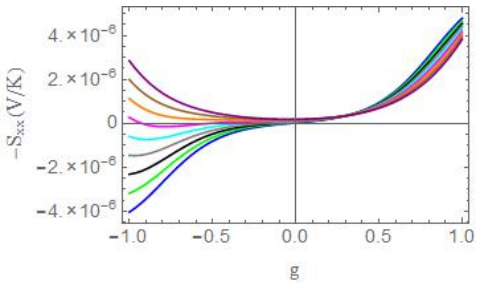

(e) $\gamma = 1.9$ and $c = 0.51$.

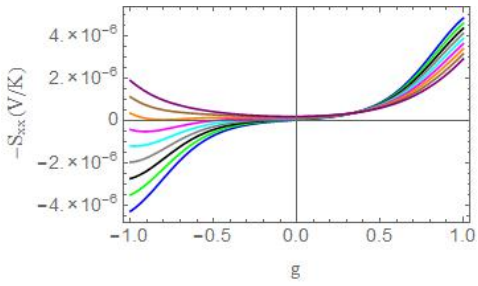

Figure 7.6: The results from the model for different γ values, where $\Delta/T = 15$.

In fig.7.6 the fan effect caused by the differing dominations can be seen once more on the extreme left of the graph, confirming that it is the bulk that is dictating the sign change. It can also be observed that the minimum value when the thermopower is curved has also lowered from that for $\Delta/T = 10$. This is to be expected as $\Delta/T = 15$ acts at a lower temperature and as such the plateau at the filling factor would be more defined. At the right of the graph, where the two regimes seem to be following the same path, it can be seen that the purple lines, which is dominated by the edge movement, changes more steeply with the varying values of γ than the bulk dominated regime does. This is due to the variation in the transition value c, which plays such a large part in the equation for the chemical potential.

7.3.3 $\Delta/T = 20$

The value of $\Delta/T = 20$ corresponds to the low temperature of approximately 20mK. This means that for this regime tunnelling will be the dominate form of particle transport. As such it is expected that the γ value required to allow the model to correctly correspond to the experimental data, will be relatively low. The model will be run once more over all the α values, as well as for $\gamma = 1.1, 1.3, 1.5, 1.7, 1.9$. The transition value will be the one that corresponds to the γ and the Δ/T values. This is shown in fig.7.7 and fig.7.8.

(a) $\gamma = 1.1$ and $c = 0.83$.

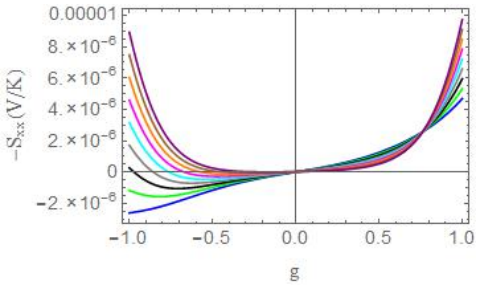

(b) $\gamma = 1.3$ and $c = 0.77$.

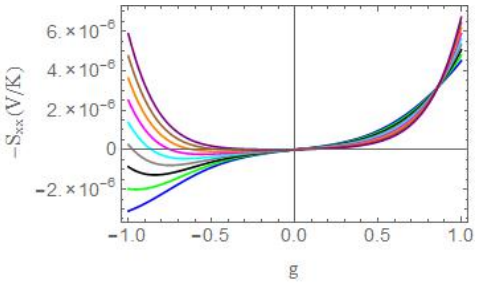

Figure 7.7: The results from the model for different γ values, where $\Delta/T = 20$.

(a) $\gamma = 1.5$ and $c = 0.70$.

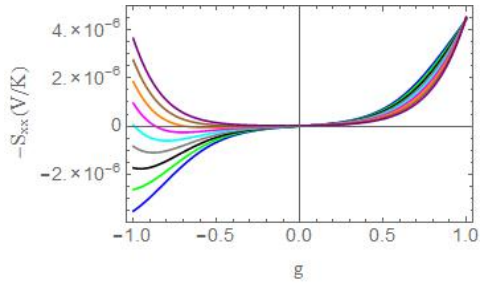

(b) $\gamma = 1.7$ and $c = 0.64$.

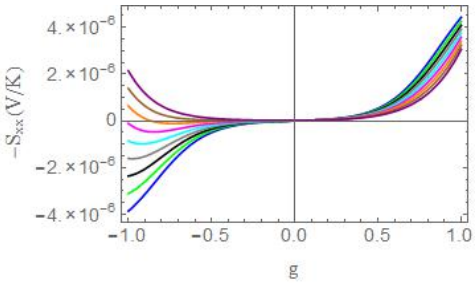

(c) $\gamma = 1.9$ and $c = 0.59$.

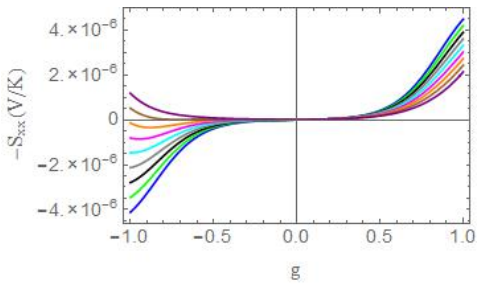

Figure 7.8: The results from the model for different γ values, where $\Delta/T = 20$.

In fig.7.8 it can be seen that there is very little difference between the graphs given by the model. This is due to the high value of γ causing the results to mimic as those from the simplified model shown earlier. Therefore due to the high value of Δ/T, and thus the low temperature, there is a limit to how much change can be seen when tunnelling is not taken as the most dominate form of transport in the system. The graphs in fig.7.7 show how the thermopower behaves when the tunnelling is taken into account. Both these graphs have the majority of the lines showing the dip to the minimum value of thermopower, which is expected at the centre of the plateau. They also show how close the lines are getting to the zero, with some of the middle values of α showing a slight change in sign, similar to that was seen in the experimental data in [3].

7.4 Comparison With Experimental Data

To compare the results obtained from the model with the experiential data, the values of the free parameters, α and γ must be decided. The values used for fig.7.9 are $\gamma = 1.5$ and $\alpha = 0.7$.

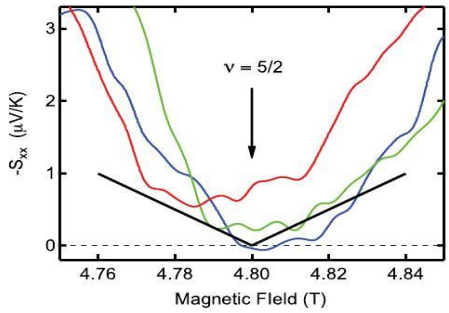

(a) Thermopower data for the 5/2 state from [3]. The black line shows a different gtheoretical prediction by Yang and halperin [40].

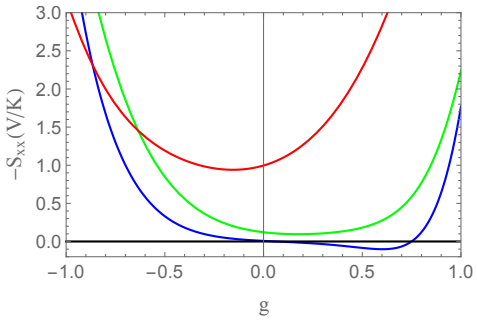

(b) Thermopower from the model that includes tunnelling with $\gamma = 1.5$ and $\alpha = 0.7$.

Figure 7.9: Plots showing how the thermopower changes with the different values of temperature for both the experimental data and the model that includes tunnelling. The different coloured lines are for the different temperatures, blue=20mK, green=28mK, and red=41mK.

From fig.7.9 it can be seen that this model is a good fit for the experimental data. The data obtained from the model is the correct order of magnitude and in good agreement of that found experimentally. It shows the reversal of sign for the thermopower as well as how it behaves for the different temperatures, including how the minima in the thermopower moves across the plateau as the temperature decreases. It shows that the inclusion of tunnelling does indeed help drive the model closer to the experimental results obtained.

Chapter 8

Conclusion and Further Work

Throughout this thesis a model to describe the behaviour of thermopower has been developed, using for its basis one designed in the Corbino geometry. The assumption that Dykhne's theorem can be used for a potential that is not asymmetric, see fig.8.1, has been tested and found correct.

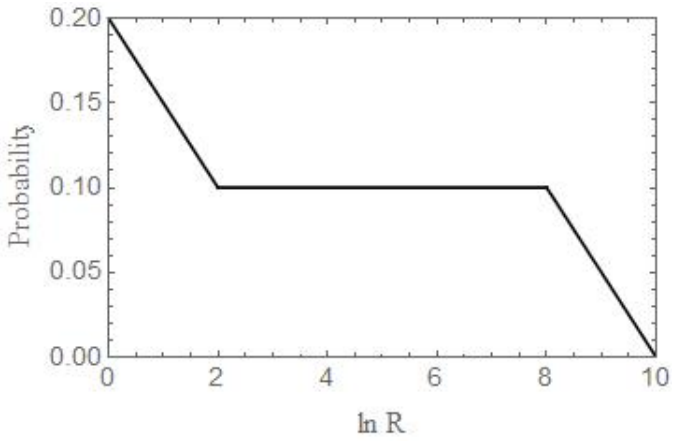

Figure 8.1: A diagram showing the asymmetric potential caused by tunnelling.

The current through the edges states has been derived to include the behaviour of the chemical potential μ. This then was combined with the model found in [6] to create a simplified model of the thermopower in a Hall bar geometry. The free parameter of the current splitting, α was investigated and a suitable value found. This result was then compared with the experimental data published in [3] to see if this model could describe the situation.

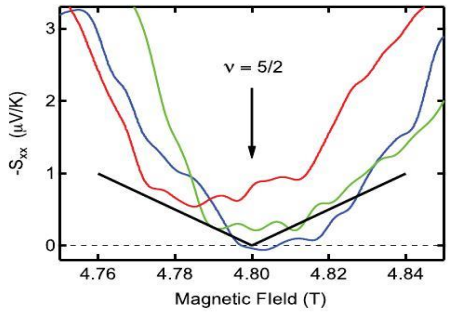

(a) Thermopower data for the 5/2 state from [3]. The black line shows a different gtheoretical prediction by Yang and halperin [40].

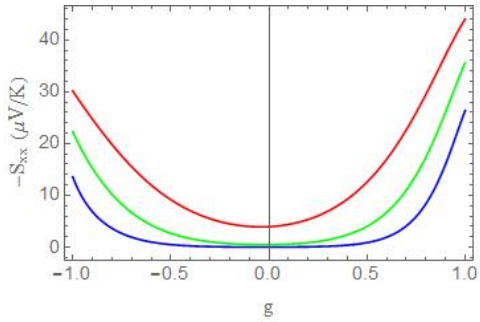

(b) Thermopower from the simplified model with $c = 0.8$ and $\alpha = 0.7$.

Figure 8.2: Plots showing how the thermopower changes with the different values of temperature for both the experimental data and the simplified model. The different coloured lines are for the different temperatures, blue=20mK, green=28mK, and red=41mK.

It was seen that this model was not complex enough to be used to explain the thermopower and as such tunnelling was included. With this addition came the tunnelling parameter γ which varies depending on the value of the temperature. This was also investigated and suitable values were found so that the result from the model could once more be compared with those from experiment. This model was found to give a good approximation to the experimental results, see fig.8.3.

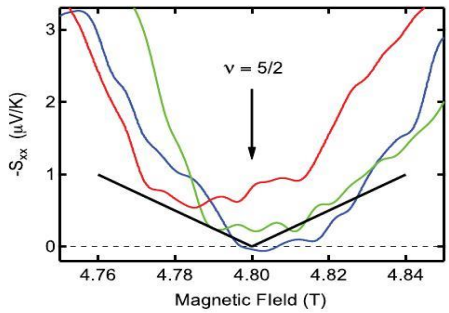

(a) Thermopower data for the 5/2 state from [3]. The black line shows a different gtheoretical prediction by Yang and halperin [40].

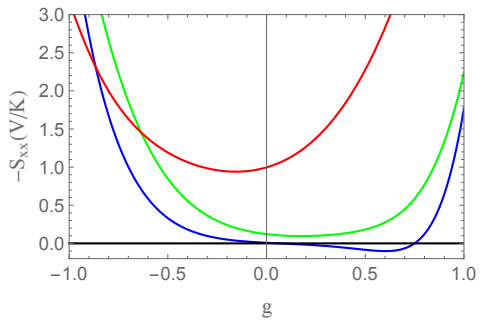

(b) Thermopower from the model that includes tunnelling with $\gamma =$ and $\alpha =$.

Figure 8.3: Plots showing how the thermopower changes with the different values of temperature for both the experimental data and the model that includes tunnelling. The different coloured lines are for the different temperatures, blue=20mK, green=28mK, and red=41mK.

The model that has been developed throughout this thesis has a dependence upon four main parameters, they are the current splitting α, the tunnelling parameter γ, the size of the energy gap Δ and the transition value c. Both Δ and c can be determined from experimental data, and from those an estimate of γ can be obtained. Therefore the only truly free parameter in this model is that of α, as it is the only one that can not be calculated from experimental data and as such must be presumed. Throughout this work that presumption was that it was a constant, but this could well not be the case.

To further develop the model discussed in this thesis, analysing how a changing α value effects the results would be an effective choice. It is suggested in [31] that the current splitting parameter α could be modelled as a capacitor, this concept could produce a more accurate description of the thermopower at low temperatures if it were to be included into the model.

Bibliography

[1] K. V. Klitzing, G. Dorda, and M. Pepper. New method for high-accuracy determination of the fine-structure constant based on quantized hall resistance. *Phys. Rev. Lett. Phys.*, 45:494, 1980.

[2] D. Yoshioka. *The Quauntum Hall Effect*. Springer, Germany, 2002.

[3] W. E. Chickering, J. P. Eisenstein, L. N. Pfeiffer, and K. W. West. Thermoelectric response of fractional quantized hall and reentrant insulating states in the n=1 landau level. *Phys. Rev. B*, 87, 075302, 2013.

[4] D. G. Polyakov and B. I. Shklovskii. Universal prefactor of activated conductivity in the quantum hall effect. *Phys. Rev. Lett.*, 74:150–153, 1995.

[5] B. Derrida and J. Vannimenus. A transfer-matrix approach to random resistor networks. *J. Phys. A: Math. Gen.*, 15:L557–L564, 1982.

[6] N. d'Ambrumenil and R. H. Morf. Thermopower in the quantum hall regime. *Phys. Rev. Lett.*, 111, 136805, 2013.

[7] Stormer H. L. Tsui, D. C. and A. C. Gossard. Two-dimensional magnetotransport in the extreme quantum limit. *Phys. Rev. Lett.*, 48:1559, 1982.

[8] David J. Griffiths. *Introducion to Electrodynamics*. Pearson Education, United States of America, 2008.

[9] J.R. Hook and H.E. Hall. *Solid State Physics*. John Wiley and Sons, Chicester, England, 2010.

[10] T Chakraborty and P Pietilainen. *The Quantum Hall Effects, Ingegral and Fractional*. Springer, Germany, 1995.

[11] Zyun F. Wzawa. *Quantum Hall Effects, Recent Theoretical and Experimental Developments*. World Scientific Publishing Co., Singapore Malaysia, 2013.

[12] Basile Verdene Jurgen Smet Vladmir Umansky Diana Mahalu Dieter Schuh Gerhard Abstreiter Jens Martin, Shahal Ilani and Amir Yacoby. Localisation pf fractionally charged quasi-particles. *Science*, 305(5686), 2004.

[13] A. F. Ioffe. Density of states of 2d electron gas and width of the plateau of iqhe. *Solid State Communications*, 65(11), 1988.

[14] R. B. Laughlin. Quantized hall conductivity in two dimensions. *Phys. Rev. B*, 23:5632–5633, 1981.

[15] Yuri M. Galperin. *Introduction to modern solid state physics.* Amazon, UK, 2015.

[16] B. I. Halperin, P. A. Lee, and N. Read. Theory of the half-filled landau level. *Phys. Rev. B*, 47:7312, 1993.

[17] R. B. Laughlin. Anomalous quantum hall effect: An incompressible quantum fluid with fractionally charged excitations. *Phys. Rev. Lett.*, 50:1395–1398, 1983.

[18] O. Heinonen. *Composite Fermions: A Unified View of the Quantum Hall Regime.* World Scientific, Singapore, 1998.

[19] B. I. Halperin. Statistics of quasiparticles and the hierarchy of fractional quantized hall states. *Phys. Rev. Lett.*, 52:1583, 1984.

[20] H. L. Strmer D. C. Tsui A. C. Gossard R. Willett, J. P. Eisenstein and J. H. English. Observation of an even-denominator quantum number in the fractional quantum hall effect. *Phys. Rev. Lett.*, 59:1776, 1987.

[21] G. Moore and N. Read. *Nucl. Phys. B*, 360, 362, 1991.

[22] W. E. Chickering. *Thermopower in Two-Dimensional Electron Systems.* PhD thesis, Californa Institute of Technology, 2016.

[23] N. R. Cooper, B. I. Halperin, and I.M. Ruzin. Thermoelectric response of an interacting two-dimensional electron gas in a quantizing magnetic field. *Phys. Rev. B*, 55:2344, 1997.

[24] B. I. Halperin Kun. Yang. Thermopower as a possible probe of non-abelian quasiparticle statistics in fractional quantum hall liquids. *Phys. Rev. B.*, 79:115317, 2009.

[25] Chong Xiao. *Synthesis and optimization of chalogenides quantum dots thermoelectric materials*. Springer, Berlin, 2016.

[26] W.E. Chickering, J.P. Eisentein, L. N. Pfeiffer, and K. W. West. Thermopower of two-dimensional electrons at filling factors $\nu = 3/2$ and $5/2$. *Phys. Rev. B*, 81:245319, 2010.

[27] Kun. Yang Yafis. Barlas. Thermopower of quantum hall states in corbino geometry as a measure of quasiparticle entropy. *Phys. Rev. B.*, 85:195107, 2012.

[28] S. Bilodeau G. Gervais L. N. Pfeiffer B. A. Schmidt, K. Bennaceur and K. W. West. Second landau level fractional quantum hall effects in the corbino geometry. *Solid State Communications*, 217:1, 2015.

[29] L. N. Pfeiffer J. P. Eisentein, K. B. Cooper and K. W. West. Insulating and fractional quantum hall states in the first excited landau level. *Phys. Rev. Lett.*, 88(7), 2002.

[30] P. Lederer M. O. Goerbig and C. Morais Smith. Microscopic theory of the reentrant integer quantum hall effect in the first and second excited lls. *Phys. Rev. B.*, 68:241302(R), 2003.

[31] B. I. Halperin. Quantized hall conductance, current-carrying edge states, and the existence of extended states in a two-dimensional disordered potential. *Phys. Rev. B*, 25:2185, 1982.

[32] A. M. Dykhne. *Sov. Phys. JETP*, 32:63, 1971.

[33] N. d'Ambrumenil, B. I. Halperin, and R. H. Morf. Model for dissipative conductance in fractional quantum hall states. *Phys. Rev. Lett.*, 106:126804, 2011.

[34] Ifan G. Hughes and Thomas P.A.Hase. *Measurements and their Uncertainties A practical guide to modern error analysis*. Oxford University Press, Oxford, 2013.

[35] David J. Griffiths. *Introduction to Electodynamics*. Pearson Benjamin Cummings, USA, 2008.

[36] David J. Griffiths. *Introduction to Quantum Mechanics*. Pearson Benjamin Cummings, USA, 2005.

[37] Rodger A. Freedman Hugh D. Young. *University Physics with Modern Physics 12th edition*. Pearson Addison Wesley, USA, 2008.

[38] R. W. van der Heijden H. van Zalinge and J. H. Wolter. Anisotropic corbino magnetothermopower in a quantum hall system. *Phys. Rev. B*, 67:165311, 2003.

[39] Akira Shuhei Kobayakawa and Yasuhiro Iye. Diffusion thermopower of quantum hall states measured in corbino geometry. *J. Phys. Soc. Jpn.*, 82:053702, 2013.

[40] K. Yang and B. I. Halperin. Thermopower as a possible probe of non-abelian quasiparticle statistics in fractional quantum hall liquids. *Phys. Rev. B*, 79:115317, 2009.

[41] H. A. Fertig and B. I. Halperin. Transmission coefficient of an electron through a saddle-point potential in a magnetic field. *Phys. Rev. B*, 36:7969–7976, 1987.